Atg5 plays crucial roles in naked mole-rat cell proliferation and maintenance of cellular homeostasis

(Atg5 はハダカデバネズミ細胞の増殖と恒常性維持に重要な役割を果たす)

A Doctoral Thesis

By

Junhyeong Kim

Department of Oncogene Research,

Research Institute for Microbial Diseases,

Osaka University

May, 2020

Contents

Abbreviations

NMR : Naked mole-rat

NSF : Naked mole-rat skin fibroblast

MEF : Mouse embryonic fibroblast

MSF : Mouse skin fibroblast

ECI : Early contact inhibition

HMM-HA : High Molecular Mass-Hyaluronan

Atg5 : Autophagy related protein 5

LC3b : Microtubule-associated protein light chain 3 beta

pRb : Retinoblastoma protein

shRNA : short hairpin RNA

HIF-1α : hypoxia inducible factor-1 alpha

p16^{INK4a} : cyclin-dependent kinase inhibitor 2A

p21^{Waf1} : cyclin-dependent kinase inhibitor 1A

p27^{Kip1} : cyclin-dependent kinase inhibitor 1B

ECI : Early Contact Inhibition

HAS2 : Hyaluronan Synthase 2

HYAL2 : Hyaluronidase 2

CQ : Chloroquine

PI : Propidium Iodide

D-PBS : Dulbecco's Phosphate-Buffered Saline

FBS : Fetal Bovine Serum

SDS-PAGE : Sodium Dodecyl Sulfate-Polyacrylamide Gel Electrophoresis

SA-β-gal : Senescence Associated-β-Galactosidase

General Introduction

1. Naked Mole Rat

The naked mole-rat (NMR, *heterocephalus glaber*) is a eusocial subterranean rodent. NMRs and Damaraland mole-rats (*Fukomys damarensis*) are only two eusocial mammalian species like eusocial insects (Jarvis, 1981; Bennett and Jarvis, 1988). Recent years, NMRs are emerging model organisms for studies on mammalian cancer and aging.

Physiological characteristics of Naked Mole Rats

1) Longevity

NMRs are known for the longest-living rodent species (Buffenstein, 2005). A maximum lifespan of NMRs is more than 30 years (Lewis and Buffenstein, 2016). While body size of NMRs is similar to that of the house mouse (*Mus musculus*), NMRs live 10 times longer than house mouse (Edrey et al., 2011). Furthermore, NMRs generally experience a greatly extended healthy lifespan within theire total lifespan of over 30 years (Buffenstein, 2008; Ruby et al., 2018). An NMR queen reproduces until death (Buffenstein and Jarvis, 2002; Buffenstein, 2008). Furthermore, NMRs show a low metabolic rate approximately 70% of that of a house mouse (Yahav and Buffenstein, 1991). Also, NMRs exhibit few age-related changes in basal metabolism (O'Connor et al., 2002; Triplett et al., 2015a). Moreover, NMRs display no age-related cardiac or vascular changes (Csiszar et al., 2007; Grimes et al., 2014). NMRs also have upregulated expression of DNA repair genes delaying aging (MacRae et al., 2015; Hoejimakers, 2009), improved proteostasis (Pride et al., 2015), and a stable epigenome (Tan et al, 2017).

2) Cancer resistance

These extraordinary animals also exhibit profound resistance to spontaneous tumorigenesis (Buffenstein, 2008). Initial case of cancer in NMRs was reported at 2016, while NMRs have been observed since 1980s (Delaney et al., 2016). NMRs are also exceptionally resistant to experimentally induced cancer (Liang et al., 2010; Seluanov et al., 2009).

3) Adaptation to hypoxia

NMRs live in colonies underground with low-oxygen environment (Lewis and Buffenstein, 2015). Therefore, NMRs can tolerate hypoxic conditions as low as 3% (Nathaniel et al., 2009). Recent study reported that NMRs can survive 18 min without apparent injury in the absence of Oxygen (Anoxia). Under anoxic conditions, NMRs switch from glucose-based anaerobic metabolism to that of fructose (Park et al., 2017). Furthermore, HIF-1α, a master regulator of mammalian O_2 homeostasis, contributes to hypoxia of adaptation to NMRs (Xiao et al., 2017).

4) Naked mole-rat cells

Fibroblasts derived from NMRs do not exhibit replicative senescence, but proliferate very slowly in culture (Seluanov et al., 2008). Several cellular level studies identified mechanisms involved in longevity and cancer resistance of NMRs. Previous study reported that proliferation of NMR fibroblasts were suppressed at a much lower cell density than mouse fibroblasts (Seluanov et al., 2009). This phenomenon, termed early contact inhibition (ECI), contributes to anti-cancer mechanisms. This study also revealed that p53 and pRb tumor suppressor pathways regulates cell cycle arrest, apoptosis and ECI in NMR fibroblasts. Interestingly, $p16^{INK4a}$ (Cyclin-dependent kinase inhibitor 2A) is also implicated in regulation of ECI in NSFs. In mammalian cells, $p16^{INK4a}$ is generally regarded as a unique and specific marker of cellular senescence and irreversible cell cycle arrest (Hernandez-Segura et al., 2018). In case of NMR fibroblasts, however, $p16^{INK4a}$ regulates reversible cell cycle arrest instead of $p27^{kip1}$ (Cyclin-dependent kinase inhibitor 1B) in a cell density-dependent manner. Thus, this study also suggested that upregulation of $p16^{INK4a}$ is not a specific marker of cellular senescence in NMR fibroblasts. Furthermore, NMR fibroblasts secrete high-molecular-mass hyaluronan (HMM-HA), which is required for ECI (Tian et al., 2013). Suppression of HAS2 (a hyaluronan synthase) or overexpression of HYAL2 (a hyaluronan-degrading enzyme) contributes to malignant transformation of NMR fibroblasts. Moreover, an additional isoform from INK4a/b locus, the $p15^{INK4b}/p16^{INK4a}$ hybrid named as $pALT^{INK4a/b}$, contributes to the cancer resistance of NMR by inducing cell cycle arrest in NSFs (Tian et al., 2015).

On the other hands, recent studies also reported that induced pluripotent stem cells (iPSCs) derived from NMR cells exhibits resistance to tumorigenesis (Miyawaki et al., 2016; Lee et al., 2017). Furthermore, suppression of ARF, a tumor suppressor gene, triggers NMR-specific cellular senescence as a safeguard against reprogramming and oncogenic transformation (Miyawaki et al., 2016). Interestingly, gene expression patterns of NMR iPSCs are more similar to those of human than mouse iPSCs (Lee et al., 2017). In addition, inactivation of pRb contributes to reprogramming of NMR cells (Tan et al., 2017).

2. Autophagy

Macroautophagy (hereafter, autophagy) is the evolutionarily conserved cellular pathway that degrades intracellular components including soluble proteins, aggregated proteins, organelles, and macromolecules via the lysosomal degradation to recycle them to maintain cellular homeostasis at basal state. Autophagy also contributes to cell survival under stress conditions, such as nutrient or growth factor deprivation, hypoxia, reactive oxygen species (ROS), DNA damage or intracellular pathogens (Levine & Kroemer, 2008).

Molecular mechanisms of autophagy

The molecular mechanism of autophagy is composed of following steps; initiation, nucleation, elongation, docking and fusion, degradation.

1) Initiation and Nucleation

Various stimuli, such as nutrient starvation, lead to the formation of isolation membrane from various organelles, including mitochondria, mitochondria-associated membranes, the Golgi complex, the endoplasmic reticulum (ER), the plasma membrane and recycling endosome (Puri et al., 2013; Hamasaki et al., 2013; Moreau et al., 2011; Ravikumar et al., 2010; Hailey et al., 2010; Axe et al., 2008;). Autophagosome formation is initiated by the ULK complex (ULK 1/2, Atg13, Atg101 and FIP200) at Atg9-containing membranes, followed by ULK1 dependent Atg9 phosphorylation (Karanasios et al., 2016). This event leads to the formation of isolation membrane and activates the class III PI3-kinase nucleation complex. (Vps34, Beclin1, Vps15 and Atg14). Activated the class III PI3-kinase nucleation complex supports formation and elongation of a double-membrane structure (the isolation memebrane or phagopore) via production of phosphatidylinositol 3-phosphpate (PI3P).

2) Elongation

The elongation of the isolation membrane/phagophore leads to the formation of double-membrane autophagosome, which is processed by two ubiquitin-like conjugation steps catalyzed by Atg7. Atg7 first conjugates Atg5 and Atg12, which them complex with Atg16L to form the Atg5-Atg12-Atg16L complex on the outer membrane of the phagophore (Glick *et al.*, 2010; Kaur & Debnath, 2015). The second step involves the processing of Atg8/LC3. When autophagy is induced, pre-Atg8/LC3 is converted to Atg8/LC3-I by Atg4 protease, and Atg8/LC3-I is conjugated to phosphatidylethanolamine (PE) by Atg7 to generate Atg8/LC3-II. Atg8/LC3-II is then recruited to the elongating phagophore dependently on the Atg12-Atg5-Atg16L complex. LC3B-II is present on both the inner and outer membrane of the autophagosome, and plays a role in the completion of the autophagosome formation. Since Atg8/LC3-II remains covalently bound to the inner membrane of autophagosome, production of Atg8/LC3-II is used as a general marker for autophagy (Mizushima et al., 2010).

3) Docking and fusion

Upon completion of autophagosome formation, PE is cleaved from LC3B-II by Atg4 on the outer membrane and the resulting LC3B-I is released to the cytosol. The matured autophagosome is then fused with primary lysosome via the lysosomal membrane protein LAMP-2 and the small GTPase Rab7, resulting in the formation of autolysosomes (Fortunato et al., 2009; Jäger et al., 2004; Gutierrez et al., 2004).

4) Degradation

In autolysosomes, the incorporated materials are completely digested by lysosomal enzymes under acidic conditions. The digested small molecules, such as amino acids, are released back to the cytosol to be re-used for protein synthesis and maintenance of cellular functions under starvation conditions.

Autophagy in aging and longevity

Many species display decreased autophagy activity with age (Nakamura et al., 2019; Chang et al., 2017; Kaushik et al., 2012; Simonsen et al., 2008; Donati et al., 2001). Also, many studies have reported that activation of autophagy is implicated in extension of lifespan in model organisms. Suppression of insulin/IGF-1 signaling (Meléndez et al., 2003), caloric restriction (Hansen et al., 2008; Jia and levine et al., 2007), and resvertrol treatment (Morselli et al., 2010) contributes to both autophagy activation and life extension of *C.elegans*. Furthermore, Rapamycin treatment (Bjedov et al., 2009), Brain-specific overexpression of Atg8a (Simonsen et al., 2008) and neuron-specific upregulation of Atg1 (Ulgherait et al., 2014) activate autophagy and extend lifespan in *Drosophila*. Moreover, Atg5 overexpression in mice contributes to activation of autophagy and extension of lifespan (Pyo et al., 2013). Recent study also reported that disruption of belin1-Bcl2 interaction activates autophagy and extends lifespan of mice (Fernández et al., 2018)

Autophagy in Naked mole-rat

Previous study showed that NMR brain tissue maintains high levels of basal autophagy for most of lifespan (Triplett et al., 2015b). Also, very young and adult NMRs display increased levels of basal autophagy compared to mouse. (Zhao et al., 2014). Inhibition of PI3K/Akt pathway activates autophagy in NMR skin fibroblasts. (Zhao et al., 2016). Furthermore, autophagy levels of leydig cell regulate the fertility of male NMRs (Yang et al., 2017). However, molecular mechanisms underlying high basal autophagy of naked mole-rats and its physiological roles remains to be elucidated.

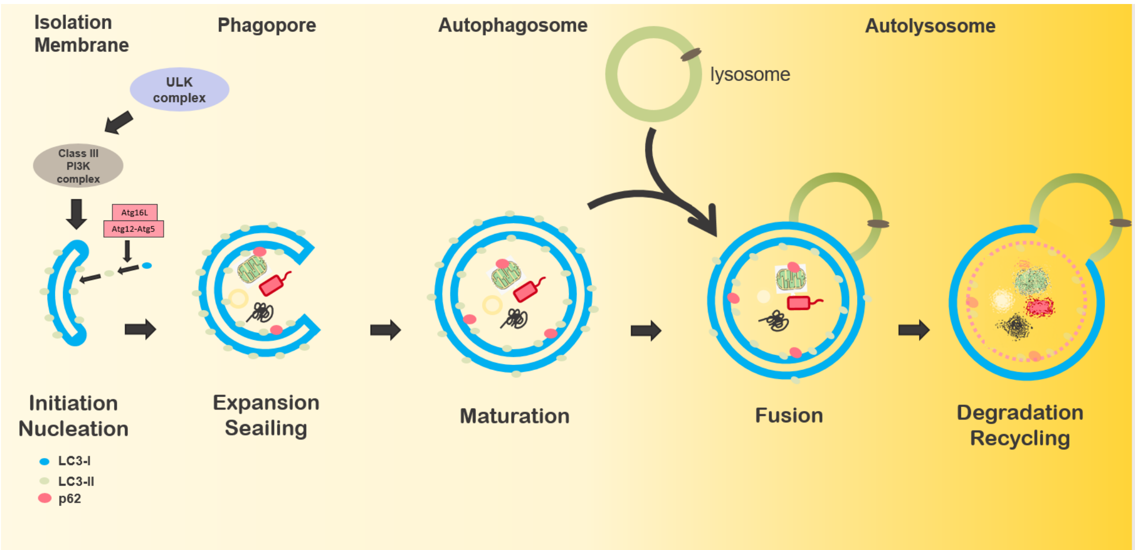

Figure. General Introduction

Molecular mechanisms of macroautophagy.

References of general introduction

Axe, E.L., Walker, S.A., Manifava, M., Chandra, P., Roderick, H.L., Habermann, A., Griffiths, G. and Ktistakis, N.T. 2008. Autophagosome formation from membrane compartments enriched in phosphatidylinositol 3-phosphate and dynamically connected to the endoplasmic reticulum. *Journal of Cell Biology*, **182**: 685–701.

Bennett, N.C., Jarvis, J.U.M. 1988. The Social Structure and Reproductive Biology of Colonies of the Mole-Rat, *Cryptomys damarensis* (Rodentia, Bathyergidae). *Journal of Mammalogy*, **69**: 293-302.

Levine, B. and Kroemer, G. 2008. Autophagy in the Pathogenesis of Disease. *Cell*, **132**: 27–42.

Bjedov, I., Toivonen, J.M., Kerr, F., Slack, C., Jacobson, J., Foley, A. and Partridge, L. 2010. Mechanisms of Life Span Extension by Rapamycin in the Fruit Fly Drosophila melanogaster. *Cell Metabolism*, **11**: 35–46.

Buffenstein, R and Jarvis, J.U.M. 2002. The naked mole rat-a new record for the oldest living rodent. *Science of Aging Knowledge Enviroment*, **2002**: pe7

Buffenstein, R. 2005. The naked mole-rat: A new long-living model for human aging research. *Journals of Gerontology - Series A Biological Sciences and Medical Sciences*, **60**: 1369–1377.

Buffenstein, R. 2008. Negligible senescence in the longest living rodent, the naked mole-rat: Insights from a successfully aging species. *Journal of Comparative Physiology B: Biochemical, Systemic, and Environmental Physiology*, **178**: 439–445.

Chang, J.T., Kumsta, C., Hellman, A.B., Adams, L.M. and Hansen, M. 2017. Spatiotemporal regulation of autophagy during Caenorhabditis elegans aging. *eLife*, **6**: 1–23.

Csiszar, A., Labinskyy, N., Orosz, Z., Xiangmin, Z., Buffenstein, R. and Ungvari, Z. 2007. Vascular aging in the longest-living rodent, the naked mole rat. *American Journal of Physiology - Heart and Circulatory Physiology*, **293**: 919–927.

Donati, A., Cavallini, G., Paradiso, C., Vittorini, S., Pollera, M., Gori, Z. and Bergamini, E. 2001. Age-related changes in the regulation of autophagic proteolysis in rat isolated hepatocytes. *Journals of Gerontology - Series A Biological Sciences and Medical Sciences*, **56**: B288–B293.

Delaney, M.A., Ward, J.M., Walsh, T.F., Chinnadurai, S.K., Kerns, K., Kinsel, M.J. and Treuting, P.M. 2016. Initial Case Reports of Cancer in Naked Mole-rats (Heterocephalus glaber). *Veterinary Pathology*, **53**: 691–696.

Edrey, Y.H., Park, T.J., Kang, H., Biney, A. and Buffenstein, R. 2011. Endocrine function and neurobiology of the longest-living rodent, the naked mole-rat. *Experimental Gerontology*, **46**: 116–123.

Fernández, Á.F., Sebti, S., Wei, Y., Zou, Z., Shi, M., McMillan, K.L., He, C., Ting, T., Liu, Y., Chiang, W.C., Marciano, D.K., Schiattarella, G.G., Bhagat, G., Moe, O.W., Hu, M.C. and Levine, B. 2018. Disruption of the beclin 1-BCL2 autophagy regulatory complex promotes longevity in mice. *Nature*, **558**: 136–140.

Fortunato, F., Bürgers, H., Bergmann, F., Rieger, P., Büchler, M.W., Kroemer, G. and Werner, J. 2009. Impaired Autolysosome Formation Correlates With Lamp-2 Depletion: Role of Apoptosis, Autophagy, and Necrosis in Pancreatitis. *Gastroenterology*, **137**: 350-360.e5.

Glick, D., Barth, S. and Macleod, K.F. 2010. Autophagy : cellular and molecular mechanisms. The Journal of Pathology, 221, 3–12. http://doi.org/10.1002/path.2697. *Journal of Pathology*, **221**: 3–12.

Grimes, K.M., Reddy, A.K., Lindsey, M.L. and Buffenstein, R. 2014. And the beat goes on: Maintained cardiovascular function during aging in the longest-lived rodent, the naked mole-rat. *American Journal of Physiology - Heart and Circulatory Physiology*, **307**: 284–291.

Gutierrez, M.G., Munafó, D.B., Berón, W. and Colombo, M.I. 2004. Rab7 is required for the normal progression of the autophagic pathway in mammalian cells. *Journal of Cell Science*, **117**: 2687–2697.

Hailey, D.W., Rambold, A.S., Satpute-Krishnan, P., Mitra, K., Sougrat, R., Kim, P.K. and Lippincott-Schwartz, J. 2010. Mitochondria Supply Membranes for

Autophagosome Biogenesis during Starvation. *Cell*, **141**: 656–667.

Hamasaki, M., Furuta, N., Matsuda, A., Nezu, A., Yamamoto, A., Fujita, N., Oomori, H., Noda, T., Haraguchi, T., Hiraoka, Y., Amano, A. and Yoshimori, T. 2013. Autophagosomes form at ER-mitochondria contact sites. *Nature*, **495**: 389–393.

Hansen, M., Chandra, A., Mitic, L.L., Onken, B., Driscoll, M. and Kenyon, C. 2008. A role for autophagy in the extension of lifespan by dietary restriction in C. elegans. *PLoS Genetics*, **4**.

Hernandez-Segura, A., Nehme, J. and Demaria, M. 2018. Hallmarks of Cellular Senescence. *Trends in Cell Biology*, **28**: 436–453.

Hoeijmakers, J.H.J. 2009. DNA Damage, Aging, and Cancer. 1475–1485.

Jäger, S., Bucci, C., Tanida, I., Ueno, T., Kominami, E., Saftig, P. and Eskelinen, E.L. 2004. Role for Rab7 in maturation of late autophagic vacuoles. *Journal of Cell Science*, **117**: 4837–4848.

Jarvis, J.U.M. 1981. Eusociality in a mammal: Cooperative breeding in naked mole-rat colonies. *Science*, **212**: 571–573.

Jia, K. and Levine, B. 2007. Autophagy is required for dietary restriction-mediated life span extension in C. elegans. *Autophagy*, **3**: 597–599.

Karanasios, E., Walker, S.A., Okkenhaug, H., Manifava, M., Hummel, E., Zimmermann, H., Ahmed, Q., Domart, M.C., Collinson, L. and Ktistakis, N.T. 2016. Autophagy initiation by ULK complex assembly on ER tubulovesicular regions marked by ATG9 vesicles. *Nature Communications*, **7**.

Kaur, J. and Debnath, J. 2015. Autophagy at the crossroads of catabolism and anabolism. *Nature Reviews Molecular Cell Biology*, **16**: 461–472.

Kaushik, S., Arias, E., Kwon, H., Lopez, N.M., Athonvarangkul, D., Sahu, S., Schwartz, G.J., Pessin, J.E. and Singh, R. 2012. Loss of autophagy in hypothalamic POMC neurons impairs lipolysis. *EMBO Reports*, **13**: 258–265.

Lee, S.G., Mikhalchenko, A.E., Yim, S.H., Lobanov, A.V., Park, J.K., Choi, K.H., Bronson, R.T., Lee, C.K., Park, T.J. and Gladyshev, V.N. 2017. Naked Mole Rat

Induced Pluripotent Stem Cells and Their Contribution to Interspecific Chimera. *Stem Cell Reports*, **9**: 1706–1720.

Lewis, K.N. and Buffenstein, R. 2015. The Naked Mole-Rat: A Resilient Rodent Model of Aging, Longevity, and Healthspan. A Resilient Rodent Model of Aging, Longevity, and Healthspan. *Handbook of the Biology of Aging: Eighth Edition*, 179–204.

Liang, S., Mele, J., Wu, Y., Buffenstein, R. and Hornsby, P.J. 2010. Resistance to experimental tumorigenesis in cells of a long-lived mammal, the naked mole-rat (Heterocephalus glaber). *Aging Cell*, **9**: 626–635.

MacRae, S.L., Croken, M.M.K., Calder, R.B., Aliper, A., Milholland, B., White, R.R., Zhavoronkov, A., Gladyshev, V.N., Seluanov, A., Gorbunova, V., Zhang, Z.D. and Vijg, J. 2015. DNA repair in species with extreme lifespan differences. *Aging*, **7**: 1171–1184.

Meléndez, A., Tallóczy, Z., Seaman, M., Eskelinen, E.L., Hall, D.H. and Levine, B. 2003. Autophagy genes are essential for dauer development and life-span extension in C. elegans. *Science*, **301**: 1387–1391.

Miyawaki, S., Kawamura, Y., Oiwa, Y., Shimizu, A., Hachiya, T., Bono, H., Koya, I., Okada, Y., Kimura, T., Tsuchiya, Y., Suzuki, S., Onishi, N., Kuzumaki, N., Matsuzaki, Y., Narita, M., Ikeda, E., Okanoya, K., Seino, K.I., Saya, H., Okano, H., Miura, K. 2016. Tumour resistance in induced pluripotent stem cells derived from naked mole-rats. *Nature Communications*, **7**: 1–9.

Mizushima, N., Yoshimori, T. and Levine, B. 2010. Methods in Mammalian Autophagy Research. *Cell*, **140**: 313–326.

Moreau, K., Ravikumar, B., Renna, M., Puri, C. and Rubinsztein, D.C. 2011. Autophagosome precursor maturation requires homotypic fusion. *Cell*, **146**: 303–317.

Morselli, E., Maiuri, M.C., Markaki, M., Megalou, E., Pasparaki, A., Palikaras, K., Criollo, A., Galluzzi, L., Malik, S.A., Vitale, I., Michaud, M., Madeo, F., Tavernarakis, N. and Kroemer, G. 2010. Caloric restriction and resveratrol promote longevity through the Sirtuin-1-dependent induction of autophagy. *Cell Death and Disease*, **1**: 1–10.

Nakamura, S., Oba, M., Suzuki, M., Takahashi, A., Yamamuro, T., Fujiwara, M., Ikenaka, K., Minami, S., Tabata, N., Yamamoto, K., Kubo, S., Tokumura, A., Akamatsu, K., Miyazaki, Y., Kawabata, T., Hamasaki, M., Fukui, K., Sango, K., Watanabe, Y., *et al.* 2019. Suppression of autophagic activity by Rubicon is a signature of aging. *Nature Communications*, **10**: 1–11.

Nathaniel, T.I., Saras, A., Umesiri, F.E. and Olajuyigbe, F. 2009. Tolerance to oxygen nutrient deprivation in the hippocampal slices of the naked mole rats. *Journal of Integrative Neuroscience*, **8**: 123–136.

O'Connor, T.P., Lee, A., Jarvis, J.U.M. and Buffenstein, R. 2002. Prolonged longevity in naked mole-rats: Age-related changes in metabolism, body composition and gastrointestinal function. *Comparative Biochemistry and Physiology - A Molecular and Integrative Physiology*, **133**: 835–842.

Park, T.J., Reznick, J., Peterson, B.L., Blass, G., Omerbašić, D., Bennett, N.C., Kuich, P.H.J.L., Zasada, C., Browe, B.M., Hamann, W., Applegate, D.T., Radke, M.H., Kosten, T., Lutermann, H., Gavaghan, V., Eigenbrod, O., Bégay, V., Amoroso, V.G., Govind, V., Minshall, R.D., Smith, E.S.J., Larson, J., Gotthardt, M., Kepma, S., Lewin, G.R. 2017. Fructose-driven glycolysis supports anoxia resistance in the naked mole-rat. *Science*, **356**: 307–311.

Pride, H., Yu, Z., Sunchu, B., Mochnick, J., Coles, A., Zhang, Y., Buffenstein, R., Hornsby, P.J., Austad, S.N. and Pérez, V.I. 2015. Long-lived species have improved proteostasis compared to phylogenetically-related shorter-lived species. *Biochemical and Biophysical Research Communications*, **457**: 669–675.

Puri, C., Renna, M., Bento, C.F., Moreau, K. and Rubinsztein, D.C. 2013. Diverse autophagosome membrane sources coalesce in recycling endosomes. *Cell*, **154**: 1285–1299.

Pyo, J.O., Yoo, S.M., Ahn, H.H., Nah, J., Hong, S.H., Kam, T.I., Jung, S. and Jung, Y.K. 2013. Overexpression of Atg5 in mice activates autophagy and extends lifespan. *Nature Communications*, **4**: 1–9.

Rodriguez, K.A., Wywial, E., Perez, V.I., Lambert, A.J., Edrey, Y.H., Lewis, K.N., Grimes, K., Lindsey, M.L., Brand, M.D. and Buffenstein, R. 2011. Walking the Oxidative Stress Tightrope: A Perspective from the Naked Mole-Rat, the Longest-Living Rodent. *Current Pharmaceutical Design*, **17**: 2290–2307.

Ravikumar, B., Moreau, K., Jahreiss, L., Puri, C. and Rubinsztein, D.C. 2010. Plasma membrane contributes to the formation of pre-autophagosomal structures. *Nature Cell Biology*, **12**: 747–757.

Ruby, J.G., Smith, M. and Buffenstein, R. 2018. Naked mole-rat mortality rates defy gompertzian laws by not increasing with age. *eLife*, **8**: 1–18.

Seluanov, A., Hine, C., Bozzella, M., Hall, A., Sasahara, T.H.C., Ribeiro, A.A.C.M., Catania, K.C., Presgraves, D.C. and Gorbunova, V. 2008. Distinct tumor suppressor mechanisms evolve in rodent species that differ in size and lifespan. *Aging Cell*, **7**: 813–823.

Seluanov, A., Hine, C., Azpurua, J., Feigenson, M., Bozzella, M., Mao, Z., Catania, K.C. and Gorbunova, V. 2009. Hypersensitivity to contact inhibition provides a clue to cancer resistance of naked mole-rat. *Proceedings of the National Academy of Sciences of the United States of America*, **106**: 19352–19357.

Simonsen, A., Cumming, R.C., Brech, A., Isakson, P., Schubert, D.R. and Finley, K.D. 2008. Promoting basal levels of autophagy in the nervous system enhances longevity and oxidant resistance in adult Drosophila. *Autophagy*, **4**: 176–184.

Tan, L., Ke, Z., Tombline, G., Macoretta, N., Hayes, K., Tian, X., Lv, R., Ablaeva, J., Gilbert, M., Bhanu, N. V., Yuan, Z.F., Garcia, B.A., Shi, Y.G., Shi, Y., Seluanov, A. and Gorbunova, V. 2017. Naked Mole Rat Cells Have a Stable Epigenome that Resists iPSC Reprogramming. *Stem Cell Reports*, **9**: 1721–1734.

Tian, X., Azpurua, J., Hine, C., Vaidya, A., Myakishev-Rempel, M., Ablaeva, J., Mao, Z., Nevo, E., Gorbunova, V. and Seluanov, A. 2013. High-molecular-mass hyaluronan mediates the cancer resistance of the naked mole rat. *Nature*, **499**: 346–349.

Tian, X., Azpurua, J., Ke, Z., Augereau, A., Zhang, Z.D., Vijg, J., Gladyshev, V.N., Gorbunova, V. and Seluanov, A. 2015. INK4 locus of the tumor-resistant rodent, the naked mole rat, expresses a functional p15/p16 hybrid isoform. *Proceedings of the National Academy of Sciences of the United States of America*, **112**: 1053–1058.

Triplett, J.C., Swomley, A., Kirk, J., Lewis, K., Orr, M., Rodriguez, K., Cai, J., Klein, J.B., Buffenstein, R. and Butterfield, D.A. 2015a. Metabolic clues to salubrious longevity in the brain of the longest-lived rodent: The naked mole-rat. *Journal of Neurochemistry*, **134**: 538–550.

Triplett, J.C., Tramutola, A., Swomley, A., Kirk, J., Grimes, K., Lewis, K., Orr, M., Rodriguez, K., Cai, J., Klein, J.B., Perluigi, M., Buffenstein, R. and Butterfield, D.A. 2015b. Age-related changes in the proteostasis network in the brain of the naked mole-rat: Implications promoting healthy longevity. *Biochimica et Biophysica Acta - Molecular Basis of Disease*, **1852**: 2213–2224.

Ulgherait, M., Rana, A., Rera, M., Graniel, J. and Walker, D.W. 2014. AMPK modulates tissue and organismal aging in a non-cell-autonomous manner. *Cell Reports*, **8**: 1767–1780.

Xiao, B., Wang, S., Yang, G., Sun, X., Zhao, S., Lin, L., Cheng, J., Yang, W., Cong, W., Sun, W., Kan, G. and Cui, S. 2017. HIF-1a contributes to Hypoxia adaptation of the naked mole rat. *Oncotarget*, **8**: 109941–109951.

Yahav, S. and Buffenstein, R. 1991. Huddling behavior facilitates homeothermy in the naked mole rat Heterocephalus glaber. *Physiological Zoology*, **64**: 871–884.

Yang, W., Li, L., Huang, X., Kan, G., Lin, L., Cheng, J., Xu, C., Sun, W., Cong, W., Zhao, S. and Cui, S. 2017. Levels of Leydig cell autophagy regulate the fertility of male naked mole-rats. *Oncotarget*, **8**: 98677–98690.

Zhao, S., Lin, L., Kan, G., Xu, Chang, Tang, Q., Yu, C., Sun, W., Cai, L., Xu, Chen and Cui, S. 2014. High autophagy in the naked mole rat may play a significant role in maintaining good health. *Cellular Physiology and Biochemistry*, **33**: 321–332.

Zhao, S., Li, L., Wang, S., Yu, C., Xiao, B., Lin, L., Cong, W., Cheng, J., Yang, W., Sun, W. and Cui, S. 2016. H2O2 treatment or serum deprivation induces autophagy and apoptosis in naked mole-rat skin fibroblasts by inhibiting the PI3K/Akt signaling pathway. *Oncotarget*, **7**: 84839–84850.

Abstract

The Naked mole-rat (NMR, *Heterocephalus glaber*) is the longest-living rodent species, with a maximum lifespan of over 30 years. NMRs exhibit negligible senescence, exceptional resistance to cancer, and high basal autophagy activity compared with mouse. The molecular mechanisms and physiological roles underlying the high autophagy activity in NMRs remain to be elucidated. I identified that the Atg12-Atg5 conjugate, a critical component of autophagosome formation, was highly expressed in NMR skin fibroblasts (NSFs) compared with that in mouse skin fibroblasts. I then generated Atg5 knockdown NSFs via lentiviral shRNA vectors to investigate the role of Atg5 in NSFs. Phenotypic analysis of Atg5 knockdown NSFs revealed that high basal autophagy activity in NSFs was associated with abundant expression of the Atg12-Atg5 conjugate. Atg5 knockdown in NSFs led to accumulation of dysfunctional mitochondria and frequent appearance of abnormally large-sized cells, and suppressed cell proliferation and cell adhesion ability, promoting anoikis/apoptosis accompanied by upregulation of apoptosis-related genes, Bax and Noxa. Furthermore, inhibition of the p53/Rb pro-apoptotic pathway with SV40 large T antigen abolished the increase in cell size, cell cycle arrest and suppression of cell adhesion, the phenotypes related to anoikis/apoptosis induced by Atg5 knockdown. Taken together, these results suggest that high basal autophagy activity in NMR cells, mediated by Atg5, contribute to suppression of apoptosis by interfering with the activation of the p53/Rb pro-apoptotic pathway, potentially via degradation of stress-inducing factors. This mechanism could benefit the longevity of NMR cells.

Introduction

The naked mole-rat (NMR, *heterocephalus glaber*) is a eusocial subterranean rodent, native to Africa (Jarvis, 1988). NMRs are the longest-living rodent species with a maximum lifespan of over 30 years (Buffenstein, 2005). While body size of NMRs is similar to that of house mouse (*Mus musculus*), NMRs live 10 times longer than house mouse (Edrey et al., 2011). Furthermore, NMRs display generally experience a greatly extended healthy lifespan within their lifespan of 30 years (Buffenstein, 2008). These extraordinary mammals also exhibit profound resistance to both spontaneous and experimentally induced cancer (Liang et al., 2010; Seluanov et al., 2009; Buffenstein, 2008). A previous study identified that NMR fibroblasts exhibit hypersensitive contact inhibition termed early contact inhibition, which is regulated by $p16^{INK4a}$, p53 and pRb pathways (Seluanov et al., 2009). Moreover, NMRs display increased levels of basal macroautophagy compared with mouse (Zhao et al., 2014).

Macroautophagy (hereafter, autophagy) is the evolutionarily conserved pathway that degrades intracellular components, including aggregated protein, organelles, macromolecules and invading pathogens via lysosomal degradation. Autophagy contributes to the maintenance of cellular homeostasis and fitness in both basal state a stressed state. Previous studies have suggested that autophagy is deeply implicated in animal aging. Many species display decreased autophagy activity with age (Nakamura et al., 2019; Chang et al., 2017; Kaushik et al., 2012; Simonsen et al., 2008; Donati et al., 2001). Furthermore, Studies in *C.elegans* have suggested that autophagy activation is implicated in lifespan extension (Morselli et al., 2010; Hansen et al., 2008; Jia and levine et al., 2007; Meléndez et al., 2003). Brain-specific overexpression of Atg8a (Simonsen et al., 2008) and neuron-specific upregulation of Atg1 (Ulgherait et al., 2014) activate and extend the lifespan in *Drosophila*. Atg5 overexpression in mice contributes to activation of autophagy and extension of lifespan (Pyo et al., 2013).

However, molecular mechanisms underlying high basal autophagy activity of NMRs and its physiological significance of this phenomenon remain to be elucidated.

In the present study, I identified that Naked mole-rat fibroblasts (NSFs) expressed higher levels of Atg12-Atg5 conjugate, a critical component of autophagosome formation, than mouse fibroblasts did. I then generated Atg5 knockdown NSFs via lentiviral shRNA vectors to investigate the role of Atg5 in NSFs. Phenotypic analyses revealed that increased levels of Atg12-Atg5 conjugate contributed to high levels of basal autophagy in NSFs. Furthermore, Atg5 knockdown in NSFs induced the accumulation of dysfunctional mitochondria, increase in cell size, and suppressed cell proliferation and adhesion to substrates, enhancing induction of apoptosis/anoikis. However, inhibition of the pro-apoptotic p53/Rb pathway with SV40 Large T antigen abolished apoptotic phenotypes induced by Atg5 knockdown. These results suggest that high basal autophagy levels in NMR cells, mediated in part by Atg5, contribute to suppression of apoptosis by inhibiting activation of the pro-apoptotic p53/Rb pathway, potentially via degradation of stress-inducing factors.

Materials and methods

Reagents and Antibodies

Anti-LC3b (D11) and anti-Atg5 (D5F5U) were purchased from Cell Signaling Technology (MA). Anti-β-tubulin (H-235), anti-Actin (C-11) and anti-Atg7 (B-9) were from Santa Cruz Biotechnology (TX). Anti-Pcna (Ab-1) was from Oncogene science (NY). Chloroquine and Hoechst33342 were purchased from Nacalai Tesque (Kyoto, Japan). Puromycin and Blasticidin S were purchased from InvivoGen (CA). Mitotracker® Green FM and Mitotracker® Orange CMTMRos were purchased from Invitrogen™ (CA). DAPGreen was purchased from Dojindo Molecular Technologies, Inc. (Kumamoto, Japan). Cyto-ID® was purchased from Enzo Life Sciences, Inc. (NY).

Cell culture

Primary NMR skin fibroblasts (NSF) were isolated from 1-to 2-year-old adult male NMRs. Mouse embryonic fibroblasts (MEFs) and mouse skin fibroblasts (MSFs) were isolated from adult male C57BL/6. MEFs and MSFs were immortalized with SV40 large T antigen. NIH/3T3 cells were purchased from American Type Culture Collection. All cells were cultured in Dulbecco's modified Eagle's medium (DMEM) supplemented with 15% FBS (Gibco, MA), 1% Antibiotic-Antimycotic Mixed Solution (Nacalai Tesque), 2mM L-glutamine (Nacalai Tesque) and 0.1 mM non-essential amino acids (NEAA; Nacalai Tesque). All cells are cultured at 32℃ in humidified atmosphere containing 5% CO_2, 3% O_2 on 0.1% gelatin-coated dishes.

Lentivirus preparation

I utilized lentiviral vectors pLKO.1-puro (Sigma Aldrich, MO) for shRNA expression and pCSII-CMV-SV40LT-IRES2-bsd for ectopic expression. An empty pLKO.1-puro was used as a shRNA negative control (shN.C.) vector. shRNA target sequences are shown in Table 1. Each plasmid and MISSION® Lentiviral Packaging Mix (Sigma Aldrich) was transfected into HEK293T cells with polyethylenimine MAX transfection reagent (Polysciences, PA), according to the manufacturer's protocol. The medium containing lentiviral particles was used for lentiviral transduction.

Lentiviral transduction

Cells were seeded in Φ 100 mm dishes (3×10^5 cells/dish) 24 h prior to lentiviral infection. On the subsequent day, cell culture medium was replaced with the medium containing lentiviral particles. After 48 h, lentivirus-containing medium was replaced with the medium containing puromycin (2 μg/ml) or blasticidin S (10 μg/ml) for drug selection.

Immunoblotting

Cells were washed with ice-cold D-PBS and lysed in RIPA buffer (20 mM Tris-HCl ph7.4, 150 mM NaCl, 1mM EDTA, 1% NP-40, 0.1% SDS, 50 mM NaF, 1mM Na_3VO_4 and Protease inhibitor cocktail), and cleared by centrifugation at 15,000 × g for 15 min. The lysate was then boiled for 5 min. Samples were separated by SDS-PAGE and transferred to a nitrocellulose or a PVDF membranes. HRP-conjugated secondary antibodies were detected with Chemi-Lumi One (Nacalai Tesque) using WSE6200H LuminoGraph 2 (ATTO, Tokyo, Japan)

Quantitative real-time PCR analysis

Total RNA was extracted from cells using Sepasol®-RNA I Super G (Nacalai Tesque), according to the manufacturer's protocol. Complementary DNA (cDNA) was synthesized by using the ReverTra Ace qRT-PCR RT Master Mix (Toyobo, Osaka, Japan) with 500 ng of total RNA. The qRT-PCR was performed in quadruplicate with THUNDERBIRD® SYBR Green qPCR Mix (Toyobo) using a QuantStudio5 real-time

PCR system (Applied Biosystems, MA). All experiments were repeated at least three times. The primer sequences are shown in Table 2.

SA-β-gal assay

Cells were seeded in a 6-well plate (2×10^4 cells/well) 48 h prior to staining. Cells were washed with cold D-PBS, before being fixed in 1 ml 0.5% glutaraldehyde, followed by incubation at 4℃ for 5 min. Cells were than stained with 2 ml freshly prepared 5-bromo-4-chloro-3-indoyl-β-galactopyranoside (X-Gal) staining solution, followed by incubation at 37℃ for 6 h. The staining was terminated by washing three times with cold D-PBS for 5 min. Color images of X-Gal-stained cells were captured with Bright-Field settings, mounted on an inverted light microscope, using a 10 × objective.

WST-8 cell proliferation Assay

Cell proliferation was measured by using a Cell counting Kit-8 (Dojindo). Cells were seeded in 96-well plates (500 cells/well). After cells had adhered to the dish, 10 μL Cell Counting Kit WST-8 reagent was added, followed by 2 h incubation at 32℃. Cell densities were then assessed using microplate reader at an absorbance of 450 nm. In the subsequent days, cell densities were measured at indicated time points.

Cell proliferation and adhesion assay by flow cytometer

Cells were seeded in 12-well plates (3×10^3 cells/well) 6 h prior to the first measurement. Cells were stained with Hoechst 33342 5 μg/ml for 30 min at 32℃. Cells were then washed twice with cold D-PBS. Cells were resuspended in 0.2 mL of D-PBS containing 2% FBS. The number of Hoechst 33342 positive cells was quantified using Attune NxT flow cytometer (Thermo Fisher Scientific). In the subsequent days, cell numbers were counted at the indicated time points.

Measurement of autophagy activity by flow cytometric analysis

Fluorescent dyes (DAPGreen and Cyto-ID®), which detect autophagic vacuoles in cytoplasm, were used as indicators of autophagy. Cells were stained with DAPGreen (Dojindo) 100 nM or Cyto-ID (Enzo Life Sciences, Inc.) for 30 min at 32℃ after treatment with or without chloroquine 20μM for 3 h. Cells were then washed twice with D-PBS, and resuspended in 0.2 mL of D-PBS containing 2% FBS. Fluorescence intensity were assessed by flow cytomeric analysis using a NxT flow cytometer (Thermo Fisher Scientific)

Measurement of mitochondrial mass by flow cytometric analysis

Cells were labeled with 5 μg/mL Hoechst 33342, 100 nM Mitotracker® Green FM and 100 nM Mitotracker® Orange CMTMRos for 30 min at 32℃. Cells were then washed twice with D-PBS. Cells were resuspended in 0.2 mL of D-PBS containing 2% FBS. Fluorescence intensity were assessed by Flow cytomeric analysis using a NxT flow cytometer (Thermo Fisher Scientific)

Annexin V-PI analysis

Cells were labeled with Annexin V-FITC and PI using Annexin V-FITC apoptosis detection kit (Nacalai Tesque), according to the manufacturer’s protocol. Fluorescence intensity was assessed by Flow cytomeric analysis using a NxT flow cytometer (Thermo Fisher Scientific).

Statistical analysis

Data were analyzed with *t*-test or one-way ANOVA followed by Dunnett’s test or Tukey’s test as indicated in figure legends. Analyses were performed using GraphPad Prism 8 (GraphPad Software) or Excel (Microsoft)

Tables

Table 1 shRNA sequences.

Target gene	Sequence
NMR-Atg5-#1	5’-CATCAATCGTAAACTCATGGA-3’
NMR-Atg5-#2	5’-CAGAAGCTATTTCGTCCTGTG-3’

Table 2 qPCR primer sequences.

Primer	Sequence	qPCR Target
NMR-Tubb-F	5’-GAAATCGTGCACATCCAGGC-3’	NMR-β-tubulin
NMR-Tubb-R	5’-ATTCGGTCCAGCTGCAGGTC-3’	
NMR-Gapdh-F	5’-CCAGAACATCATCCCAGCGT-3’	NMR-Gapdh
NMR-Gapdh-R	5’-GTCAGATCCACCACGGACAC-3’	
NMR-Pcna-F	5’-CGATACTTACCGCTGCGACC-3’	NMR-Pcna
NMR-Pcna-R	5’-ATGATGTCTTCGTTGCCAGC-3’	
NMR-Ink4a-F	5’-TGGACTCGTGGGGCGAAAAG-3’	NMR-p16/INK4a
NMR-Ink4a-R	5’-CTTGGGTGTTGCCCATCATCA-3’	
NMR-p21-F	5’-CTTGTGCCTCGGTCTTCTGA-3’	NMR-p21/Waf1
NMR-p21-R	5’-GGCGCTTGGAGTGGTAGAAA-3	
NMR-Bax-F	5’-CCCCGAGAGGTCTTTTTCCG-3’	NMR-Bax
NMR-Bax-R	5’-TTGGTACACAGCGCCTTGAG-3’	
NMR-Noxa-F	5’-AAGGTGTGTAAGGGCACGCA-3’	NMR-Noxa
NMR-Noxa-R	5’-AGGCATCTCTCCAAGTATCGC-3’	

Results

Naked mole-rats skin fibroblasts exhibit higher basal autophagy activity and levels of the Atg12-Atg5 conjugate than mouse fibroblasts

To compare the basal autophagy activity flux among mouse NIH3T3 cells, Mouse Embryonic Fibroblasts (MEFs) and Mouse Skin Fibroblasts (MSFs), and Naked mole-rat Skin Fibroblasts (NSFs), I first assessed LC3b-II levels in these cells by immunoblotting. LC3 conversion (LC3-I to LC3-II) is an essential step for autophagosome formation during autophagy (Ichimura et al., 2000). The treatment of Chloroquine (CQ) induces the accumulation of undegraded autophagosomes via blocking autophagosome-lysosome fusion (Mauthe et al., 2018). Thus, LC3b-II accumulation is indicative of autophagy activity when lysosomal degradation is blocked by lysosomal inhibitors, such as CQ (Mizushima et al., 2010). The results showed that NSFs had substantially higher LC3b-II level than mouse fibroblasts, particularly when treated with CQ (Fig. 1A). Furthermore, I confirmed basal autophagy activity by flow cytometric analysis using DAPGreen, which detects autophagic vacuoles (Iwashita et al., 2018). Consistent with the immunoblotting data, the results showed that NSFs exhibited higher basal autophagy activity than MSFs (Fig. 1B). Interestingly, I also identified that levels of the Atg12-Atg5 conjugate were increased in NSFs relative to mouse fibroblasts, while Atg7 was expressed almost equally among cell lines (Fig. 1C). The Atg12-Atg5 conjugate is a component of Atg12-Atg5/Atg16L1 complex, which is essential for autophagosome formation (Mizushima et al., 2001). Overexpression of the Atg12-Atg5 conjugate upregulates basal autophagy levels and extends lifespan in mice (Pyo et al., 2013). Hence, I concluded that the high basal autophagy activity in NSFs was related to increased levels of the Atg12-Atg5 conjugate.

High basal autophagy in NSFs was associated with abundant Atg12-Atg5 conjugate

To examine this possibility that high levels of the Atg12-Atg5 conjugate contribute to high basal autophagy activity in NSFs, I generated Atg5 knockdown NSFs (shAtg5 NSFs) using lentiviral shRNA vectors (Fig. 2A). Transduction of lentiviral shAtg5 vectors in NSFs successfully downregulated the Atg12-Atg5 conjugated expression (Fig. 2B). I then assessed LC3b levels by immunoblot analysis in negative-control shRNA-treated NSFs (shN.C. NSF) and shAtg5 NSFs. The results showed that shAtg5 NSFs had lower levels of LC3b-II expression and higher levels of LC3b-I expression than those of shN.C. NSFs (Fig. 2C). The increase in LC3b-I and the decrease in LC3b-II is a typical phenotype of Atg5-deficient cells (Kuma, et al., 2004). Moreover, I confirmed basal autophagy activity by flow cytometric analysis with Cyto-ID, which detects autophagic vacuoles like DAPGreen. The results revealed that basal autophagy activity was efficiently decreased in shAtg5 NSFs compared to shN.C. NSFs either in the presence or absence of CQ (Fig. 2D). These results demonstrate that increased autophagic activity in NSFs was likely attributable to increased Atg12-Atg5 conjugate.

Atg5 knockdown induced the accumulation of dysfunctional mitochondria

To elucidate the role of Atg5 in NSFs, I next investigated other phenotypes of shAtg5 NSFs, which are related to maintenance of cellular homeostasis. A previous study reported that dysfunctional mitochondria are increased in Atg5-defecient MEFs (Tal et al., 2009). Therefore, I examined whether Atg5 knockdown could induces the accumulation of dysfunctional mitochondria in NSFs. Dysfunctional mitochondrial mass was indirectly assessed by measuring total and functional mitochondrial mass. I used two types of mitochondria-specific dyes that stain either total mitochondria (Mitotoracker Green FM) and functional mitochondria (Mitotracker Orange CMTMRos). Flow cytometric analyses using these dyes revealed that total mitochondrial mass was increased in Atg5-defecient MEFs, while functional mitochondrial mass was more moderately increased. These results indicated that dysfunctional mitochondria were accumulated by Atg5 ablation (Fig. 3A), consistent with the previous report (Tal et al., 2009). Similar results were obtained in NSFs. Atg5 knockdown in NSFs robustly increased total mitochondrial mass, while functional mitochondrial mass was only moderately increased (Fig. 3B). Dot plot analyses also demonstrated that Atg5 knockdown increased cell populations containing relatively more dysfunctional mitochondria over 3-fold (Fig. 3C). Taken together, these findings indicate that Atg5 knockdown in NSFs induced the accumulation of dysfunctional mitochondria, potentially reflecting the reduction of Atg5-mediated mitophagy

Atg5 knockdown produced abnormally large-sized cells

On the other hands, I noticed that abnormally enlarged cells frequently emerged in shAtg5 NSFs at 2 weeks after lentiviral shRNA transduction (Fig. 4A), while Atg5 KO MEFs exhibited no significant change in cell morphology (Fig. 4B). Previous study reported that Atg5-depleted MEF displayed slightly increased cell size (Hosokawa et al., 2006). However, shAtg5 NSFs displayed over 2-fold increase in the surface area compared with shN.C. NSFs at 2 weeks after lentiviral shRNA transduction, while Atg5-depleted MEFs showed only about 1.14-fold increase in the surface area compared to WT MEFs (Fig. 4C and 4D). I further evaluated cell volume by assessing the FSC-A using a flow cytometer. The results revealed that Atg5 knockdown in NSFs induced a greater increase in cell volume than in MEFs (Fig. 4E and 4F). In addition to increase in average cell sizes, shAtg5 NSFs displayed wider distribution of cell sizes, indicating that shAtg5 NSFs failed to maintain the uniformity of cell size. These findings suggest that Atg5 is involved in the maintenance of cell-size homeostasis in NSFs.

Atg5 knockdown induced growth arrest via p16 upregulation

Generally, suppression of genes involved in autophagy, such as Atg5, promotes cell proliferation in mouse fibroblasts (Qiang et al., 2014; Hwang et al., 2018). Indeed, Atg5 KO MEF exhibited significantly increased cell proliferation compared with WT MEFs (Fig 5A). Contrastingly, shAtg5 NSFs exhibited substantially decreased cell proliferation compared with shN.C. NSFs (Fig. 5B). Consistently, mRNA and protein levels of Pcna, a marker of cell proliferation, were downregulated by Atg5 knockdown in NSFs (Fig. 5C and 5D). Previous study reported that $p16^{Ink4a}$ is a key regulator of cell proliferation instead of $p27^{Kip1}$ in NSFs, while $p16^{Ink4a}$ generally induces an irreversible cell cycle arrest, i.e., cellular senescence, in other mammalian cells (Seluanov et al., 2009). Therefore, I compared the expression levels of $p16^{Ink4a}$ in shN.C. and shAtg5 NSFs. The qRT-PCR analysis revealed that mRNA levels of $p16^{Ink4a}$ were significantly upregulated in shAtg5 NSFs.

Atg5 knockdown did not induce cellular senescence

The observed phenotypes of shAtg5 NSFs, i.e., enlarged cell size, cell cycle arrest and upregulation of $p16^{Ink4a}$, are typical features of senescent cells (Hernandez-Segura et al., 2018). To verify a possibility whether Atg5 knockdown induced cellular senescence in NSFs, we measured the activity of senescence-associated-β-galactosidase (SA-β-gal). It is known that β-galactosidase catalyzes the hydrolysis of β-galactosides into monosaccharides only in senescent cells (Dimri et al., 1995). The results showed that the ratios of SA-β-gal positive cells were not significantly different between shN.C. NSFs and shAtg5 NSFs (Fig. 6A and 6B). Furthermore, mRNA levels of $p21^{Waf1}$, another marker of cellular senescence (Campisi et al., 2007), was not upregulated in shAtg5 NSFs (Fig. 6C). These results suggest that Atg5-depleted NSFs are likely to be quiescent cells, rather than senescent cells.

Atg5 knockdown inhibited cell adhesion, which was associated promotion of apoptosis/anoikis

Furthermore, I recognized that a high number of suspended cells were observed when shAtg5 NSFs were replated to culture dishes during subculture. I thus quantitatively compared cell adhesion ability after cell plating in shN.C. and shAtg NSFs. Cell adhesion assay revealed that cell adhesion ability was significantly decreased in shAtg5 relative to shN.C. NSFs, although depletion of Atg5 in MEFs did not affect cell adhesion ability (Fig. 7A and 7B). Previous studies reported that NSFs cannot grow under anchorage-independent conditions (Seluanov et al., 2009; Tian et al., 2013). Hence, I assessed the ratios of apoptotic cells in adherent and suspended NSFs by flow cytometric analysis using Annexin V-PI, which detects apoptotic cells. As expected, apoptotic cells were greatly increased when NSFs were suspended (Fig. 7C), indicating that NSFs undergo anoikis under this condition. Notably, Atg5 knockdown in NSFs more efficiently induced apoptosis in both adherent and suspended cells. Consistently, transcriptional levels of Bax and Noxa, pro-apoptotic factors downstream of p53, were significantly upregulated in suspended cells. These findings suggest that Atg5 knockdown attenuated cell adhesion, potentially by promoting apoptosis/anoikis, a type of programmed cell death that occurs when anchorage-dependent cells are detached from the extracellular matrix (ECM) (Frisch and Screaton, 2001), and that the pro-apoptotic p53/Rb pathway may be involved in these process

The p53/Rb pathway was required for Atg5 knockdown-induced growth arrest and induction of apoptosis/anoikis

Previous studies demonstrated that the transduction of SV40 Large T antigen (SV40 LT) abolishes cell cycle arrest at a low cell density (Early Contact Inhibtion) and inhibits apoptosis by inactivating p53/Rb pathway in NSFs (Seluanov et al., 2009; Tian et al., 2013). To elucidate the mechanistic link between Atg5 and apoptosis/anoiks, I examined the effects of inhibition of the p53/Rb pathway by SV40 LT expression on cell cycle arrest and apoptosis/anoikis in Atg5 knockdown NSFs. To do this, I stably expressed SV40 LT in NSFs via lentiviral overexpression vectors, and then transduced the cells with lentiviral shRNA vectors to generate shN.C. SV40 NSFs and shAtg5 SV40 NSFs. Immunoblot analysis was used to confirm successful successful knockdown of Atg5 (Fig. 8A) and LC3b-II levels were downregulated by Atg5 knockdown in SV40 NSFs (Fig. 8B). Furthermore, flow cytometeric analyses revealed that Atg5 knockdown in SV40 NSFs induced accumulation of dysfunctional mitochondria (Fig. 8C-E), as observed in shAtg5 NSFs (Fig. 3A-D). These results indicated that inhibition of p53/Rb by SV40 LT did not affect the basal autophagy mediated by Atg5.

However, the expression of SV40 LT suppressed other phenotypes induced by Atg5 knockdown in NSFs. For example, Atg5 knockdown in SV40 NSFs failed to produce abnormally large-sized cells and exhibited almost the same morphology as shN.C. SV40 NSFs (Fig. 8E). Moreover, shAtg5 SV40 NSFs had comparable cell proliferation rate with that of shN.C. SV40 NSFs (Fig. 8F), and cell adhesion ability was restored by the expression of SV40 LT (Fig. 8G). These results indicated that inhibition of the p53/Rb pathway by SV40 abolished cell enlargement, growth arrest, and anoikis induction, the prominent phenotypes induced by Atg5 knockdown. This in turn suggests that the p53/Rb pathway can be activated by Atg5 knockdown to induce phenotypes related to growth arrest and apoptosis, and that Atg5-mediated active autophagy may play roles in suppressing the activation of p53/Rb pathway via degradation of stress-inducing factors.

Discussion

In this study, I found that high basal autophagy activity was attributable to increased levels of the Atg12-Atg5 conjugate in skin fibroblasts derived from NMRs, which are longest-lived rodent. To address the molecular mechanisms and physiological roles of the basal Atg5-mediated autophagy in NMR cells, I examined the impact of Atg5 knockdown on the cellular phenotypes of NSFs. Atg5 knockdown induced various phenotypic changes, including robust suppression of autophagosome formation, accumulation of dysfunctional mitochondria, production of abnormally large-sized cells, growth arrest via p16 upregulation, suppression of cell adhesion, and promotion of apoptosis/anoikis via upregulation of pro-apoptotic genes. These observations underscore the crucial role for basal Atg5-mediated autophagy in the regulation of cell growth and apoptosis in NMR cells under physiological conditions (Fig. 9).

The close association between autophagy and apoptosis in NMR cells prompted me to investigate the mechanistic link between these cellular events. For this, I introduced SV40 LT in NSFs to inactivate both p53 and Rb, which are tumor suppressors acting as pro-apoptotic factors even in NMR cells. Previous studies reported that inactivation of p53/Rb with SV40 LT abolishes cell cycle arrest at a low cell density and inhibits apoptosis NSFs (Seluanov et al., 2009). In this study, I found that expression of SV40 LT did not affect the autophagy-related phenotypes induced by Atg5 knockdown, such as impaired autophagosome formation and accumulation of dysfunctional mitochondria. However, SV40 LT expression restored the uniformity of cell size, cellular proliferation and cell adhesion ability, the phenotypes closely related to apoptosis. These findings suggest that p53/Rb pathway was required for apoptosis/anoikis induced by Atg5 knockdown in NSFs, and in turn that Atg5-medated autophagy may play roles in suppressing the activation of the p53/Rb pathway which is known to be activated via various stress signals (Dick and Rubin, 2013; Sullivan et al.,

2018) in NMRs. NMRs live in a horrible environment, therefore their cells are exposed to various stressful materials, including pathogenic microbes and viruses, which are incorporated into cells. (Lewis and Buffenstein, 2015) Furthermore, long lived cells produce various stress-inducing biomaterials, such as dysfunctional organelles, denatured proteins, fatty acid peroxide, fragmented DNA/RNA, reactive oxygen species, and hypoxia, accumulation of which activate p53/Rb leading to induction of apoptosis (White, 2016; Rufini et al., 2013; Ohtani et al., 2004). Therefore, to survive under such harsh conditions for long periods, NMR may need to potentiate the Atg5-mediated autophagy to efficiently scavenge such unwanted materials to suppress p53/Rb activation. Further analysis of the molecular link between autophagy and p53/Rb activation need to be undertaken to elucidate these possibilities.

It is reported that suppression of genes involved in the activation of autophagy promotes cell proliferation in mouse fibroblasts (Qiang et al., 2014; Hwang et al., 2018). Indeed, I confirmed that Atg5 KO MEF exhibited a significantly increased cell proliferation compared with WT MEFs. In contrast, I found that Atg5 knockdown in NSFs significantly suppressed cell proliferation and even induced apoptosis. Although the molecular mechanisms underlying the functional difference between NMR and other rodents must await further study, this sharp contrast highlights the critical role of autophagy in NMRs. Since Atg5 overexpression in mice contributes to activation of autophagy and extension of lifespan (Pyo et al., 2013), the upregulation of the Atg12-Atg5 conjugate in NMRs may play a key role in the determination of longevity of NMR.

I observed that Atg5 knockdown in NSFs promoted anoikis, a type of apoptosis that occurs when cells are detached from ECM (Frisch and Screaton, 2001). Anoikis is an important anti-cancer mechanism preventing metastasis of cancer cells (Paoli et al., 2013). Previous studies demonstrated that NMR fibroblasts cannot grow under the anchorage-independent condition. Even the combination expression of oncogenic Ras and SV40 large T is not even sufficient to confer anchorage-independent growth to NMR fibroblasts. Additional transductions, such as overexpression of hTERT or HYAL2 and suppression of HAS2, are required for NMR fibroblasts to grow under the anchorage-independent condition and transform into malignant cells (Tian et al., 2015; Tian et al., 2013; Liang et al, 2010; Seluanov et al., 2009). These results indicate that NMR cells are basically highly resistant to anchorage-independent growth. In this study, I demonstrated that activation of p53/Rb pathway by Atg5 knockdown could promotes anoikis. This further implies that anoikis could be used to quickly clear damaged or aged cells in NMRs, downstream of p53 activation by diverse mechanisms. This mechanism could be beneficial in the maintenance of tissues homeostasis and prevent carcinogenesis in NMRs.

In summary, I identified Atg5-mediated autophagy as a critical regulatory mechanism for apoptosis and cellular homeostasis in NMR cells under normal conditions. These findings yield new mechanistic insights into intervention-based research seeking treatments for cancer and aging-related conditions.

References

Buffenstein, R. 2005. The naked mole-rat: A new long-living model for human aging research. *Journals of Gerontology - Series A Biological Sciences and Medical Sciences*, **60**: 1369–1377.

Buffenstein, R. 2008. Negligible senescence in the longest living rodent, the naked mole-rat: Insights from a successfully aging species. *Journal of Comparative Physiology B: Biochemical, Systemic, and Environmental Physiology*, **178**: 439–445.

Campisi, J. and D'Adda Di Fagagna, F. 2007. Cellular senescence: When bad things happen to good cells. *Nature Reviews Molecular Cell Biology*, **8**: 729–740.

Chang, J.T., Kumsta, C., Hellman, A.B., Adams, L.M. and Hansen, M. 2017. Spatiotemporal regulation of autophagy during Caenorhabditis elegans aging. *eLife*, **6**: 1–23.

Dick, F.A. and Rubin, S.M. 2013. Molecular mechanisms underlying RB protein function. *Nature Reviews Molecular Cell Biology*, **14**: 297–306.

Dimri, G.P., Lee, X., Basile, G., Acosta, M., Scott, G., Roskelley, C., Medrano, E.E., Linskens, M., Rubelj, I., Pereira-Smith, O., Peacocke, M. and Campisi, J. 1995. A biomarker that identifies senescent human cells in culture and in aging skin in vivo. *Proceedings of the National Academy of Sciences of the United States of America*, **92**: 9363–9367.

Donati, A., Cavallini, G., Paradiso, C., Vittorini, S., Pollera, M., Gori, Z. and Bergamini, E. 2001. Age-related changes in the regulation of autophagic proteolysis in rat isolated hepatocytes. *Journals of Gerontology - Series A Biological Sciences and Medical Sciences*, **56**: B288–B293.

Edrey, Y.H., Park, T.J., Kang, H., Biney, A. and Buffenstein, R. 2011. Endocrine function and neurobiology of the longest-living rodent, the naked mole-rat. *Experimental Gerontology*, **46**: 116–123.

Frisch, S.M. and Screaton, R.A. 2001. Anoikis mechanisms. *Current Opinion in Cell Biology*, **13**: 555–562.

Hansen, M., Chandra, A., Mitic, L.L., Onken, B., Driscoll, M. and Kenyon, C. 2008. A role for autophagy in the extension of lifespan by dietary restriction in C. elegans. *PLoS Genetics*, **4**.

Hernandez-Segura, A., Nehme, J. and Demaria, M. 2018. Hallmarks of Cellular Senescence. *Trends in Cell Biology*, **28**: 436–453.

Hosokawa, N., Hara, Y. and Mizushima, N. 2006. Generation of cell lines with tetracycline-regulated autophagy and a role for autophagy in controlling cell size. *FEBS Letters*, **580**: 2623–2629.

Hwang, S.H., Han, B.I. and Lee, M. 2018. Knockout of ATG5 leads to malignant cell transformation and resistance to Src family kinase inhibitor PP2. *Journal of Cellular Physiology*, **233**: 506–515.

Ichimura, Y., Kirisako, T., Takao, T., Satomi, Y., Shimonishi, Y., Ishihara, N., Mizushima, N., Tanida, I., Kominami, E., Ohsumi, M., Noda, T. and Ohsumi, Y. 2000. A ubiquitin-like system mediates protein lipidation. *Nature*, **408**: 488–492.

Iwashita, H., Sakurai, H.T., Nagahora, N., Ishiyama, M., Shioji, K., Sasamoto, K., Okuma, K., Shimizu, S. and Ueno, Y. 2018. Small fluorescent molecules for monitoring autophagic flux. *FEBS Letters*, **592**: 559–567.

Jarvis, J.U.M. 1981. Eusociality in a mammal: Cooperative breeding in naked mole-rat colonies. *Science*, **212**: 571–573.

Jia, K. and Levine, B. 2007. Autophagy is required for dietary restriction-mediated life span extension in C. elegans. *Autophagy*, **3**: 597–599.

Kaushik, S., Arias, E., Kwon, H., Lopez, N.M., Athonvarangkul, D., Sahu, S., Schwartz, G.J., Pessin, J.E. and Singh, R. 2012. Loss of autophagy in hypothalamic POMC neurons impairs lipolysis. *EMBO Reports*, **13**: 258–265.

Kuma, A., Hatano, M., Matsui, M., Yamamoto, A., Nakaya, H., Yoshimori, T., Ohsumi, Y., Tokuhisa, T. and Mizushima, N. 2004. The role of autophagy during the early neonatal starvation period. *Nature*, **432**: 1032–1036.

Lewis, K.N. and Buffenstein, R. 2015. The Naked Mole-Rat: A Resilient Rodent Model of Aging, Longevity, and Healthspan. A Resilient Rodent Model of Aging, Longevity, and Healthspan. *Handbook of the Biology of Aging: Eighth Edition*, 179–204.

Liang, S., Mele, J., Wu, Y., Buffenstein, R. and Hornsby, P.J. 2010. Resistance to experimental tumorigenesis in cells of a long-lived mammal, the naked mole-rat (Heterocephalus glaber). *Aging Cell*, **9**: 626–635.

Mauthe, M., Orhon, I., Rocchi, C., Zhou, X., Luhr, M., Hijlkema, K.J., Coppes, R.P., Engedal, N., Mari, M. and Reggiori, F. 2018. Chloroquine inhibits autophagic flux by decreasing autophagosome-lysosome fusion. *Autophagy*, **14**: 1435–1455.

Meléndez, A., Tallóczy, Z., Seaman, M., Eskelinen, E.L., Hall, D.H. and Levine, B. 2003. Autophagy genes are essential for dauer development and life-span extension in C. elegans. *Science*, **301**: 1387–1391.

Mizushima, N., Yamamoto, A., Hatano, M., Kobayashi, Y., Kabey, Y., Suzuki, K., Tokuhis, T., Ohsumi, Y. and Yoshimori, T. 2001. Dissection of autophagosome formation using Apg5-deficient mouse embryonic stem cells. *Journal of Cell Biology*, **152**: 657–667.

Mizushima, N., Yoshimori, T. and Levine, B. 2010. Methods in Mammalian Autophagy Research. *Cell*, **140**: 313–326.

Morselli, E., Maiuri, M.C., Markaki, M., Megalou, E., Pasparaki, A., Palikaras, K., Criollo, A., Galluzzi, L., Malik, S.A., Vitale, I., Michaud, M., Madeo, F., Tavernarakis, N. and Kroemer, G. 2010. Caloric restriction and resveratrol promote longevity through the Sirtuin-1-dependent induction of autophagy. *Cell Death and Disease*, **1**: 1–10.

Nakamura, S., Oba, M., Suzuki, M., Takahashi, A., Yamamuro, T., Fujiwara, M., Ikenaka, K., Minami, S., Tabata, N., Yamamoto, K., Kubo, S., Tokumura, A., Akamatsu, K., Miyazaki, Y., Kawabata, T., Hamasaki, M., Fukui, K., Sango, K., Watanabe, Y., *et al.* 2019. Suppression of autophagic activity by Rubicon is a signature of aging. *Nature Communications*, **10**: 1–11.

Ohtani, N. 2004. The p16INK4a-RB pathway: molecular link between cellular senescense and tumor suppression. *The Journal of Medical Investigation*, **51**: 146–153.

Paoli, P., Giannoni, E. and Chiarugi, P. 2013. Anoikis molecular pathways and its role in cancer progression. *Biochimica et Biophysica Acta - Molecular Cell Research*, **1833**: 3481–3498.

Pyo, J.O., Yoo, S.M., Ahn, H.H., Nah, J., Hong, S.H., Kam, T.I., Jung, S. and Jung, Y.K. 2013. Overexpression of Atg5 in mice activates autophagy and extends lifespan. *Nature Communications*, **4**: 1–9.

Rufini, A., Tucci, P., Celardo, I. and Melino, G. 2013. Senescence and aging: The critical roles of p53. *Oncogene*, **32**: 5129–5143.

Seluanov, A., Hine, C., Azpurua, J., Feigenson, M., Bozzella, M., Mao, Z., Catania, K.C. and Gorbunova, V. 2009. Hypersensitivity to contact inhibition provides a clue to cancer resistance of naked mole-rat. *Proceedings of the National Academy of Sciences of the United States of America*, **106**: 19352–19357.

Simonsen, A., Cumming, R.C., Brech, A., Isakson, P., Schubert, D.R. and Finley, K.D. 2008. Promoting basal levels of autophagy in the nervous system enhances longevity and oxidant resistance in adult Drosophila. *Autophagy*, **4**: 176–184.

Sullivan, K.D., Galbraith, M.D., Andrysik, Z. and Espinosa, J.M. 2018. Mechanisms of transcriptional regulation by p53. *Cell Death and Differentiation*, **25**: 133–143.

Tal, M.C., Sasai, M., Lee, H.K., Yordy, B., Shadel, G.S. and Iwasaki, A. 2009. Absence of autophagy results in reactive oxygen species-dependent amplification of RLR signaling. *Proceedings of the National Academy of Sciences of the United States of America*, **106**: 2774–2775.

Tian, X., Azpurua, J., Hine, C., Vaidya, A., Myakishev-Rempel, M., Ablaeva, J., Mao, Z., Nevo, E., Gorbunova, V. and Seluanov, A. 2013. High-molecular-mass hyaluronan mediates the cancer resistance of the naked mole rat. *Nature*, **499**: 346–349.

Tian, X., Azpurua, J., Ke, Z., Augereau, A., Zhang, Z.D., Vijg, J., Gladyshev, V.N., Gorbunova, V. and Seluanov, A. 2015. INK4 locus of the tumor-resistant rodent, the naked mole rat, expresses a functional p15/p16 hybrid isoform. *Proceedings of the National Academy of Sciences of the United States of America*, **112**: 1053–1058.

Ulgherait, M., Rana, A., Rera, M., Graniel, J. and Walker, D.W. 2014. AMPK modulates tissue and organismal aging in a non-cell-autonomous manner. *Cell Reports*, **8**: 1767–1780.

White, E. 2016. Autophagy and p53. *Cold spring Harbor Perspectives in Medicine*, **6**:a0 26120

Qiang, L., Zhao, B., Ming, M., Wang, N., He, T.C., Hwang, S., Thorburn, A. and He, Y.Y. 2014. Regulation of cell proliferation and migration by p62 through stabilization of Twist1. *Proceedings of the National Academy of Sciences of the United States of America*, **111**: 9241–9246.

Zhao, S., Lin, L., Kan, G., Xu, Chang, Tang, Q., Yu, C., Sun, W., Cai, L., Xu, Chen and Cui, S. 2014. High autophagy in the naked mole rat may play a significant role in maintaining good health. *Cellular Physiology and Biochemistry*, **33**: 321–332.

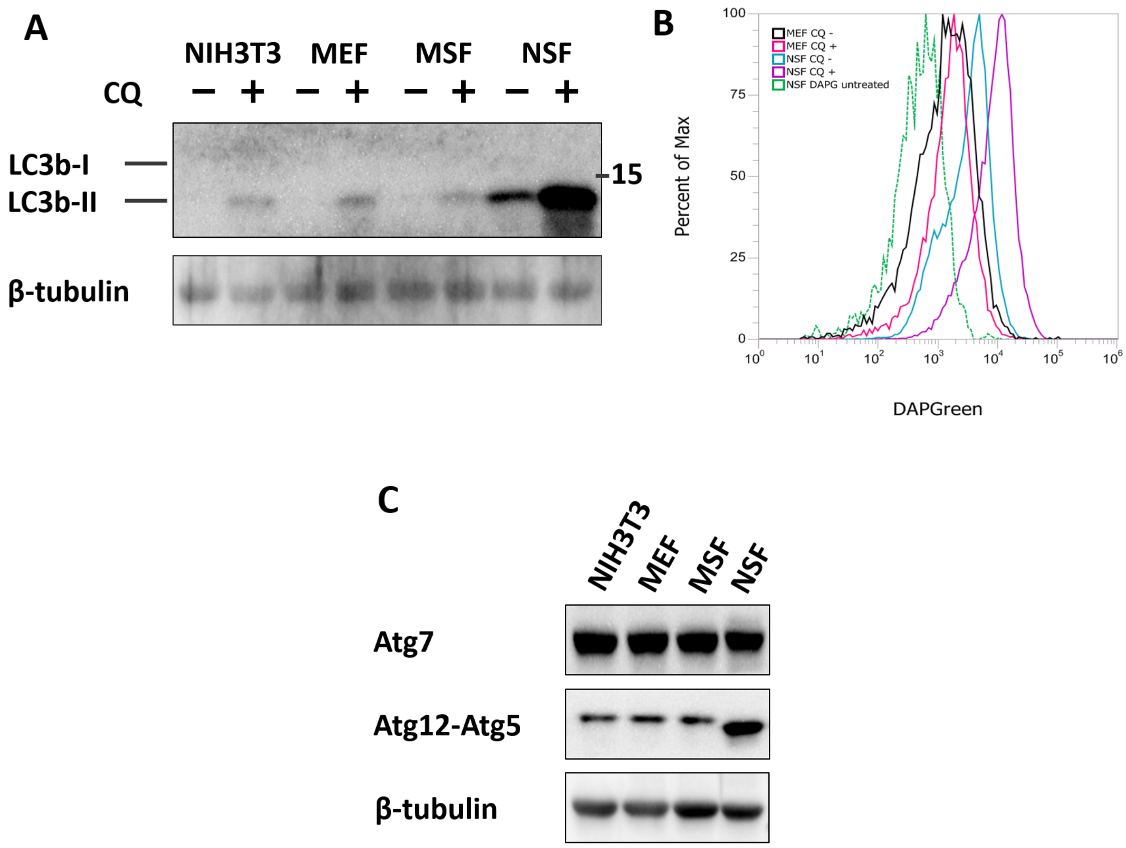

Fig. 1: NSFs exhibit higher basal autophagy activity and levels of Atg12-Atg5 conjugate expression than mouse fibroblasts.

(A) Immunoblots of LC3b expression in mouse fibroblasts and Naked mole-rat skin fibroblasts. Cells were treated with or without 20 µM CQ for 2 h prior to harvest. **(B)** Representative histogram of flow cytometric analyses showing fluorescent intensity of DAPGreen, which detects autophagic vacuoles. Cells were stained with 100 nM DAPGreen for 30 min after treatment with or without 20 µM CQ for 3 h. **(C)** Immunoblots of Atg12-Atg5 levels in mouse fibroblasts and naked mole-rat skin fibroblasts.

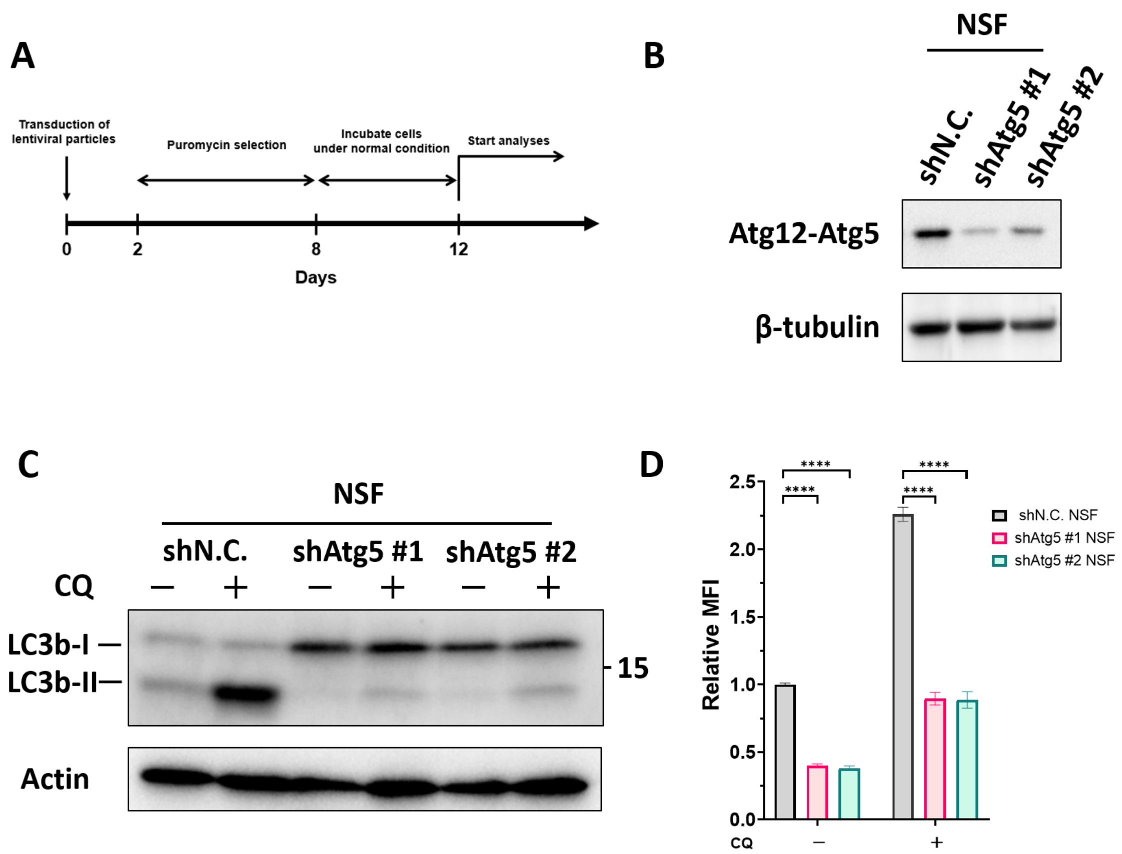

Fig. 2: Atg5 knockdown induced inactivation of autophagy in NSFs.

(A) Experimental design for Atg5 knockdown via lentiviral shRNA vectors in NSFs. Following all analyses are performed after at least 2 weeks from lentiviral transduction. **(B)** Immunoblots of the Atg12-Atg5 conjugate levels in shN.C. and shAtg5 NSFs **(C)** Immunoblots of LC3b expression in shN.C. and shAtg5 NSFs. Cells were treated with or without 20 μM CQ for 2 h. **(D)** Relative Mean Fluorescence Intensity (MFI) comparisons. Cells were labeled with Cyto-ID for 30 min, which detects autophagic vacuoles, after treatment with or without 20 μM CQ for 3 h. Values represent means ± SD of triplicates from one of three independent experiments. **** *P* <0.0001, *P* value was determined by one-way ANOVA with Dunnett's test

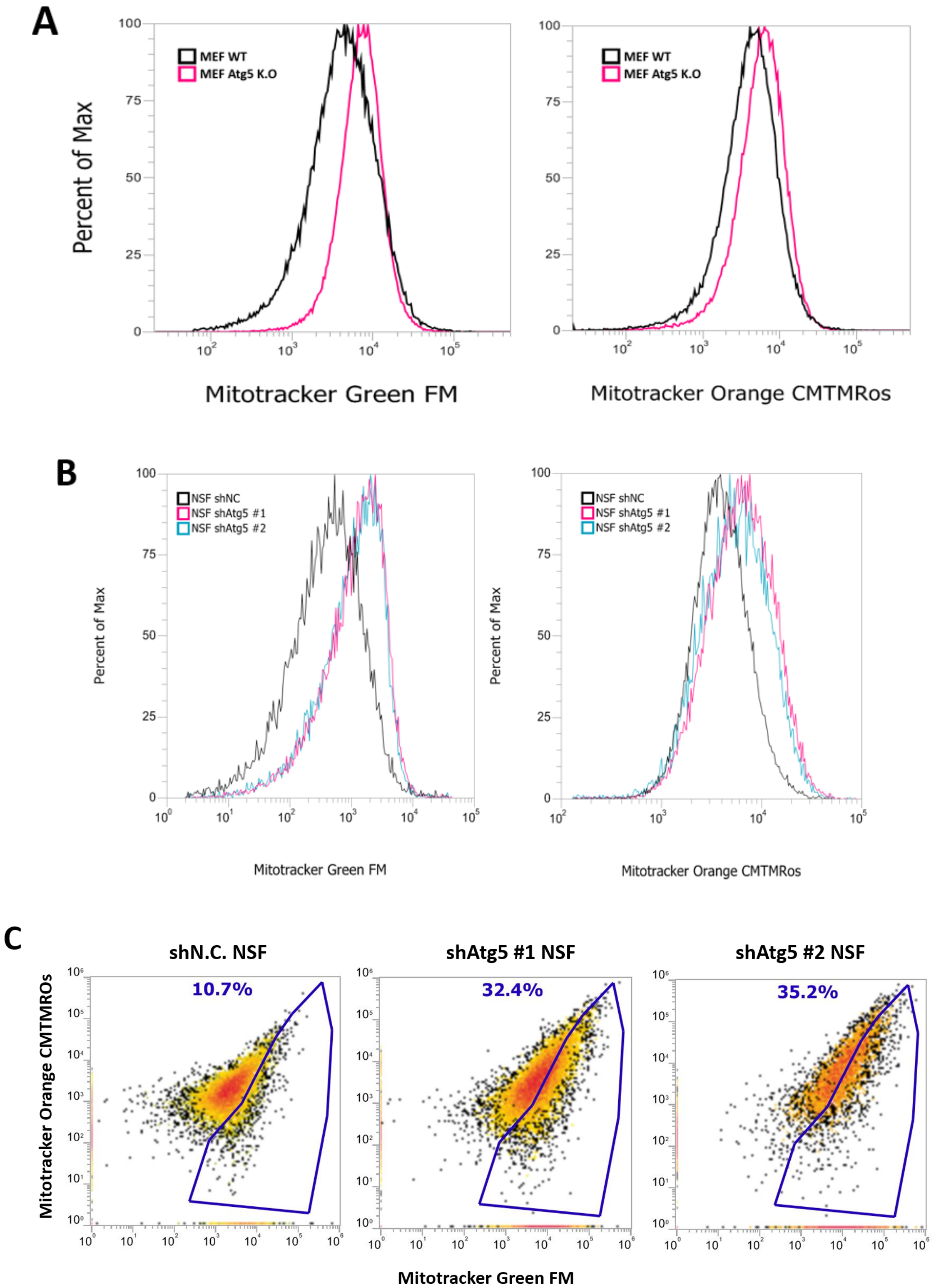
A
Percent of Max
MEF WT
MEF Atg5 K.O
Mitotracker Green FM
Mitotracker Orange CMTMRos
B
NSF shNC
NSF shAtg5 #1
NSF shAtg5 #2
Percent of Max
Mitotracker Green FM
Mitotracker Orange CMTMRos
C
shN.C. NSF
shAtg5 #1 NSF
shAtg5 #2 NSF
10.7%
32.4%
35.2%
Mitotracker Orange CMTMROs
Mitotracker Green FM

Fig. 3: Atg5 knockdown induced the accumulation of dysfunctional mitochondria.

Cells were stained with 5 μg/mL Hoechst 33342, 100 nM Mitotracker Green FM and 100 nM Mitotracker Orange CMTMRos for 30 min. **(A)** Representative histograms of flow cytometric analyses showing Mitotracker Green FM fluorescence intensity (left) and Orange CMTMRos (Right) in Wild Type (WT) and Atg5 K.O MEFs **(B)** Representative histograms of flow cytometric analysis showing Mitotracker Green FM fluorescence intensity (left) and Orange CMTMRos (Right) in shN.C. and shAtg5 NSFs. **(C)** Representative dot plots of flow cytometric analysis showing Mitotracker Green FM and Mitotracker Orange CMTMRos in shN.C. and shAtg5 NSFs. Gated regions show cell population containing relatively more dysfunctional mitochondria

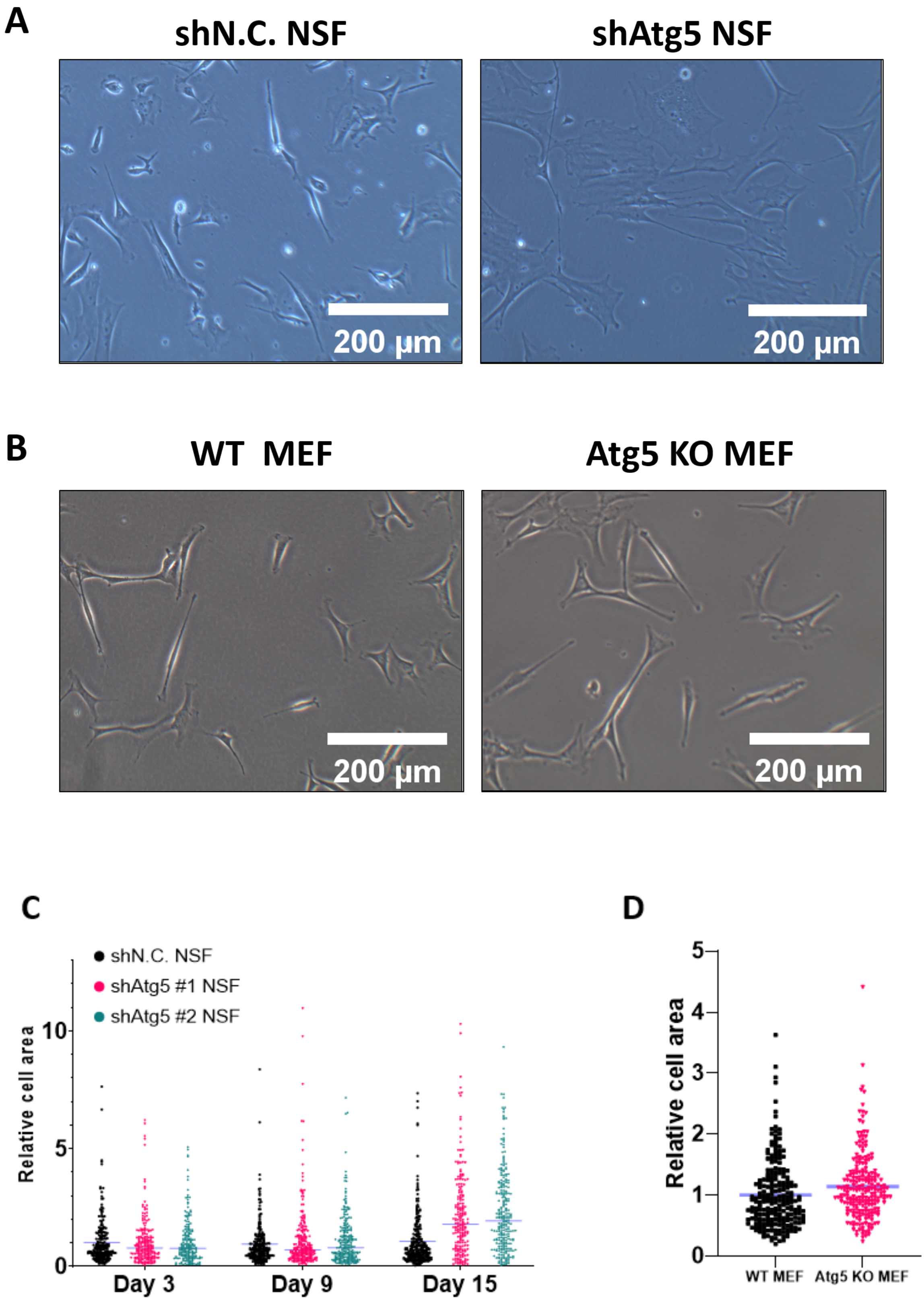
A
shN.C. NSF
shAtg5 NSF
200 μm
200 μm
B
WT MEF
Atg5 KO MEF
200 μm
200 μm
C
shN.C. NSF
shAtg5 #1 NSF
shAtg5 #2 NSF
Relative cell area
0
5
10
Day 3
Day 9
Day 15
D
Relative cell area
0
1
2
3
4
5
WT MEF
Atg5 KO MEF

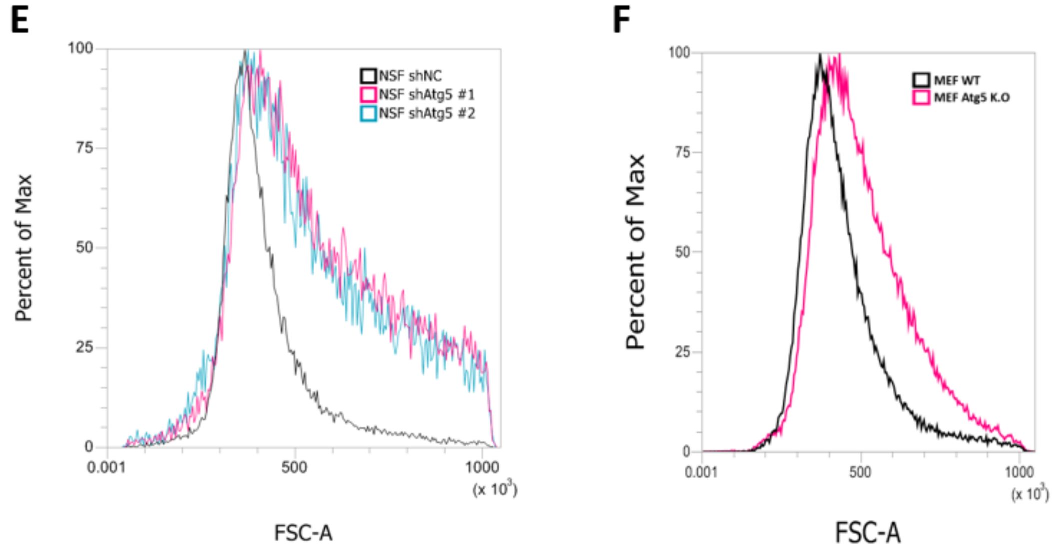

Fig. 4: Atg5 knockdown produced abnormally large-sized cells

(A) Representative images showing morphology of shN.C. and shAtg5 NSFs. **(B)** Representative images showing morphology of MEF WT and MEF Atg5 KO. Scale bars; 200 μm **(C)** Cell surface area comparsions among shN.C. and shAtg5 NSFs over the indicated time course. Lentiviral shRNA transduction was performed at Day 0. (n > 200) **(D)** Cell surface area comparison between WT and Atg5 K.O MEF. (n > 200) Horizontal bars indicate mean. **(E)** Representative FSC-A Histogram of shN.C. NSFs and shAtg5 NSFs **(F)** Representative FSC-A Histogram of WT MEFs and Atg5 KO MEFs.

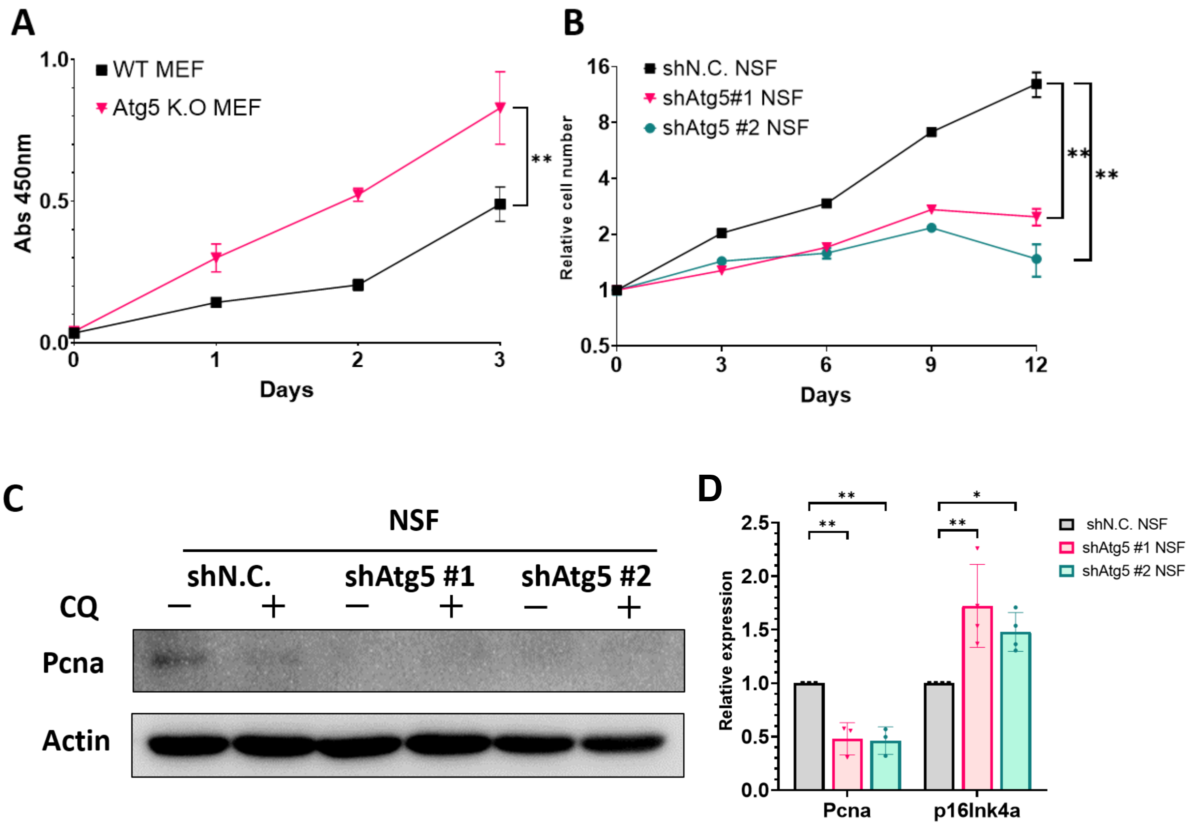

Fig. 5: Atg5 knockdown induced growth arrest via p16 upregulation

(A) Cell proliferation of WT and Atg5 K.O MEFs, as analyzed by the WST-8 growth assay over the indicated time course. Values represent means ± SD of pentaplicates from one of three independent experiments. **(B)** Cell proliferation of shN.C. and shAtg5 NSFs analyzed by FACS analysis. Cells were stained with 5 µg/mL Hoechst 33342 for 30 min. Values represent means ± SD of quadruplicates from one of three independent experiments. **(C)** Immunoblots of Pcna expression in shN.C. and shAtg5 NSFs. Cells were treated with or without 20 µM CQ for 2 h. **(D)** qRT-PCR analysis of gene expression of Pcna and $p16^{INK4a}$ in shN.C. and shAtg5 NSFs. Values represent means ± SD of at least three independent experiments. β-tubulin was used as a reference gene * *P* <0.05, ** *P* <0.01, *** *P* <0.001. *P* value was determined by Student t-test **(A)** and One-way ANOVA with Dunnett's test **(B, D)**.

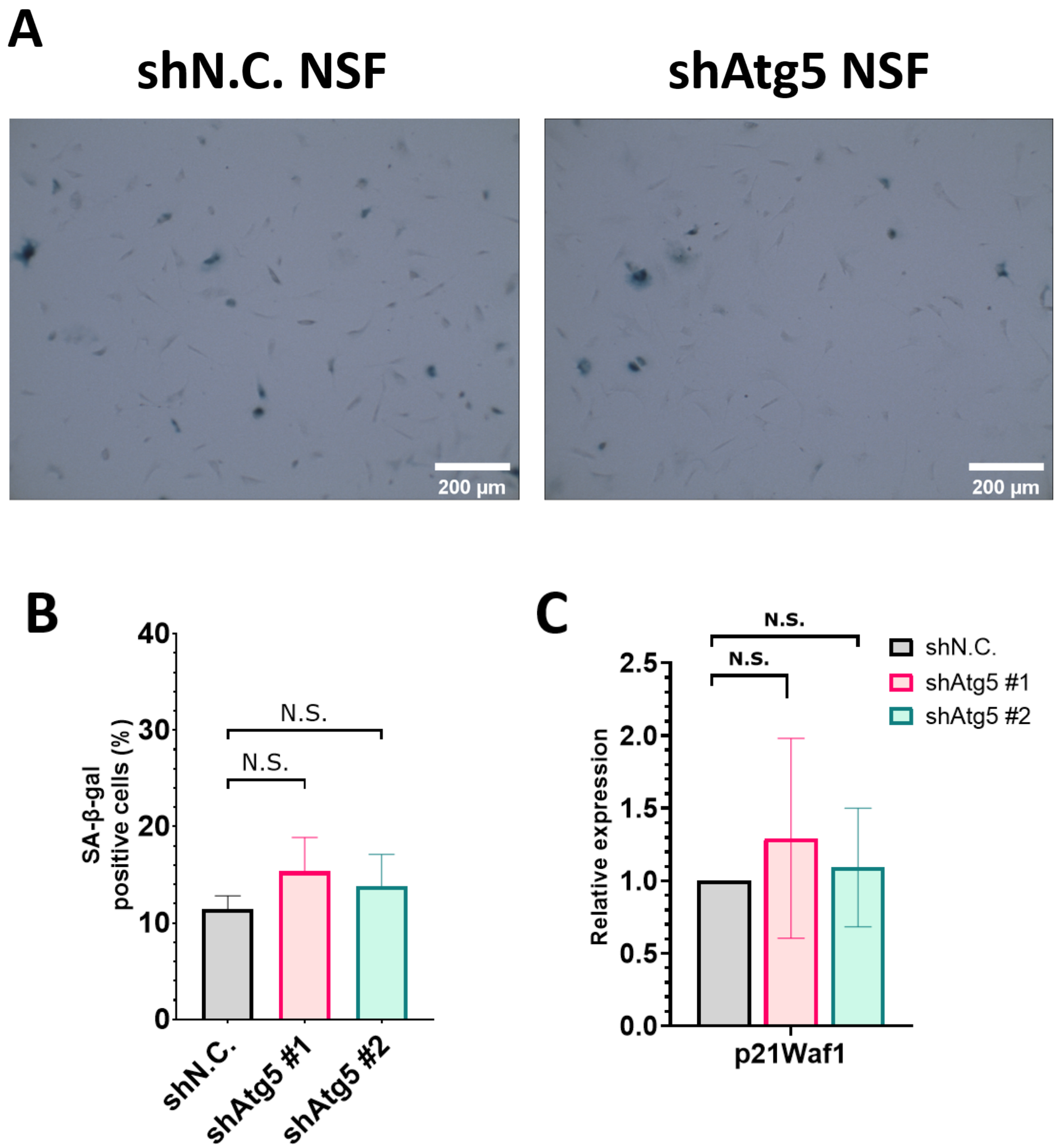

Fig. 6: Atg5 knockdown did not induce cellular senescence

(A) Representative images of SA-β-gal assay in shN.C. and shAtg5 NSFs. scale bars; 200 μm **(B)** Comparisons of SA-β-gal positive cells in shN.C. and shAtg5 NSFs. Values represent means ± SD of at least three independent experiments **(C)** qRT-PCR analysis of the expression of $p21^{Waf1}$ in shN.C. and shAtg5 NSFs. Values represent means ± SD of at least three independent experiments. N.S., not significant; *P*-value was determined by one-way ANOVA with Dunnett's test

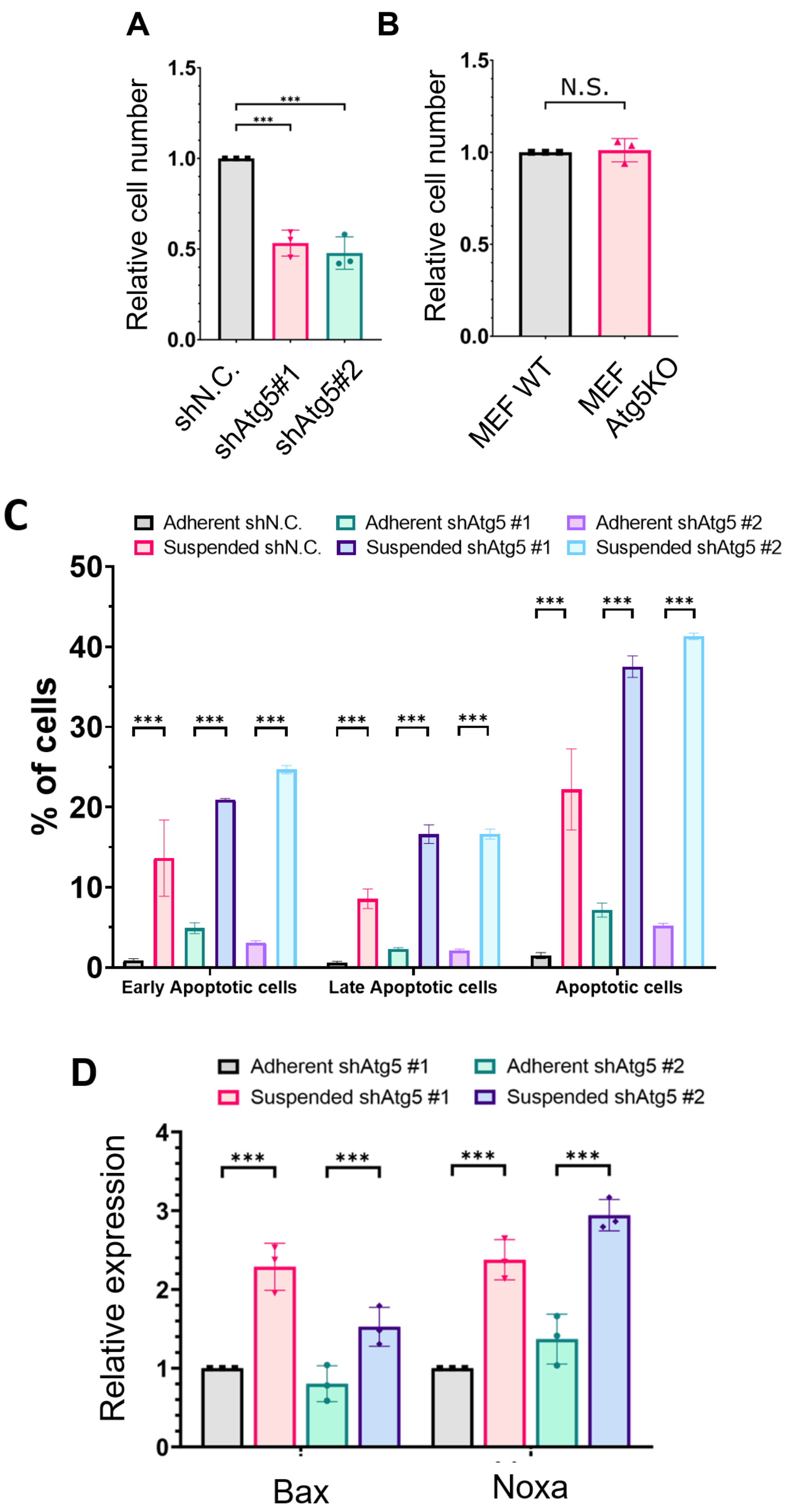
A
B
Relative cell number
1.5
1.0
0.5
0.0
***
***
shN.C.
shAtg5#1
shAtg5#2
N.S.
MEF WT
MEF Atg5KO
C
Adherent shN.C.
Suspended shN.C.
Adherent shAtg5 #1
Suspended shAtg5 #1
Adherent shAtg5 #2
Suspended shAtg5 #2
% of cells
50
40
30
20
10
0
Early Apoptotic cells
Late Apoptotic cells
Apoptotic cells
D
Adherent shAtg5 #1
Suspended shAtg5 #1
Adherent shAtg5 #2
Suspended shAtg5 #2
Relative expression
4
3
2
1
0
Bax
Noxa

Fig. 7: Atg5 knockdown inhibited cell adhesion associated with promotion of apoptosis/anoikis (A) Relative cell adhesion abilities of shN.C. NSFs and shAtg5 NSFs. **(B)** Relative cell adhesion abilities of WT MEFs and Atg5 KO MEFs **(C)** Annexin V-PI analysis of adherent and suspended NSFs. **(D)** qRT-PCR quantification of Bax and Noxa expressions in adherent and suspended shAtg5 NSFs. Values represent means ± SD of at least three independent experiments. N.S., not significant; * P <0.05 ** P <0.01 *** P <0.001, P-value was determined by one-way ANOVA with Dunnett's test **(A)**, Student t-test **(B)**, one-way ANOVA with Tukey's test **(C, D)**.

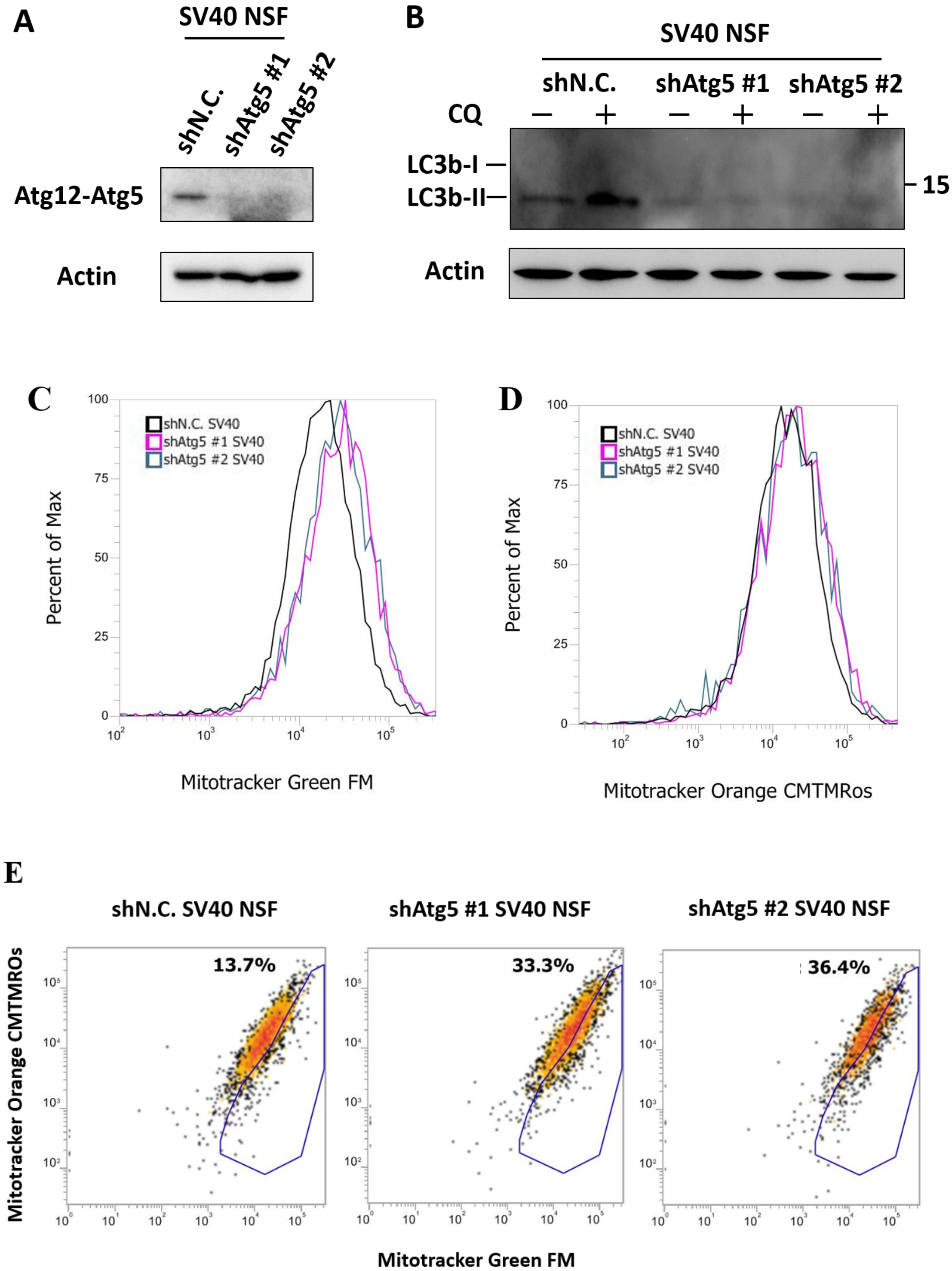
A
SV40 NSF
shN.C.
shAtg5 #1
shAtg5 #2
Atg12-Atg5
Actin
B
SV40 NSF
shN.C.
shAtg5 #1
shAtg5 #2
CQ
LC3b-I
LC3b-II
15
Actin
C
shN.C. SV40
shAtg5 #1 SV40
shAtg5 #2 SV40
Percent of Max
Mitotracker Green FM
D
shN.C. SV40
shAtg5 #1 SV40
shAtg5 #2 SV40
Percent of Max
Mitotracker Orange CMTMRos
E
shN.C. SV40 NSF
shAtg5 #1 SV40 NSF
shAtg5 #2 SV40 NSF
13.7%
33.3%
36.4%
Mitotracker Orange CMTMROs
Mitotracker Green FM

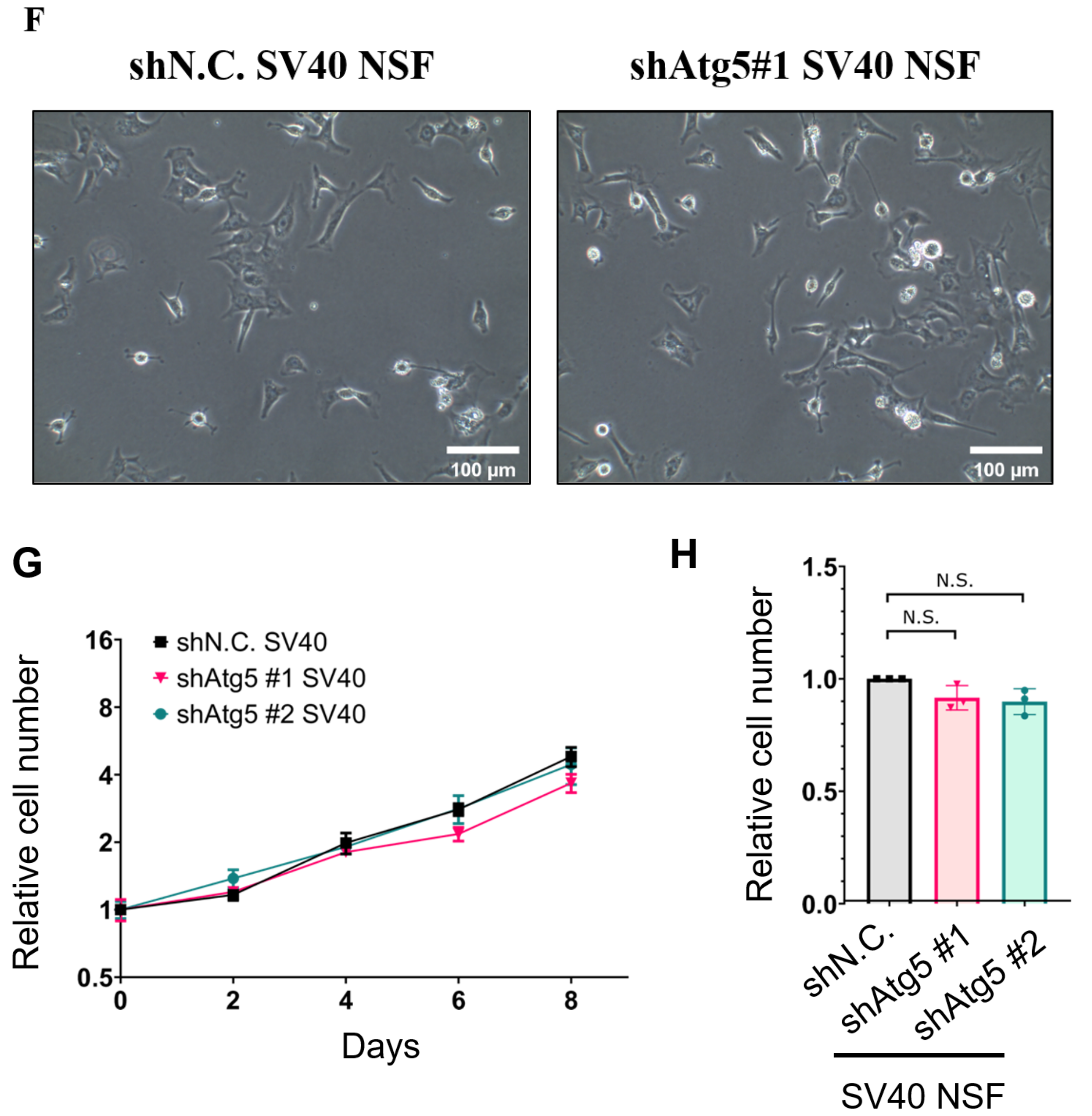

Fig. 8: The p53/Rb pro-apoptotic pathway was required for Atg5 knockdown-induced growth arrest and induction of apoptosis/anoikis.

(A) Immunoblots of Atg5 expression in shN.C. SV40 NSFs and shAtg5 SV40 NSFs. **(B)** Immunoblots of LC3b expression in shN.C. SV40 NSFs and shAtg5 SV40 NSFs. Cells were treated with or without 20 μM CQ for 2 h. **(C)** Representative histogram of Mitotracker Green FM fluorescence intensity in shN.C. SV40 NSFs and shAtg5 SV40 NSFs. **(D)** Representative histogram of Mitotracker Orange CMTMRos fluorescence intensity in shN.C. SV40 NSFs and shAtg5 SV40 NSFs. **(E)** Representative Dot plots of flow cytometric analyses showing Mitotracker Green FM and Mitotracker Orange CMTMRos. Cells were stained with 5 μg/mL Hoechst 33342, 100 nM Mitotracker

Green FM and 100 nM Mitotracker Orange CMTMRos for 30 min. Gated regions show cell populations containing relatively more dysfunctional mitochondira **(F)** Representative images showing morpology of shN.C. SV40 NSFs and shAtg5 SV40 NSFs at 2 weeks after lentiviral shRNA trasnduction. **(G)** Cell proliferation of shN.C. SV40 NSFs and shAtg5 SV40 NSFs was analyzed by flow cytometeric analysis. Cells were stained with 5 µg/mL Hoechst 33342 for 30 min. **(H)** Relative adhesion abilities of shN.C. SV40 NSFs and shAtg5 SV40 NSFs. N.S., not significant; *P*-value was determined by one-way ANOVA with Dunnett's test.

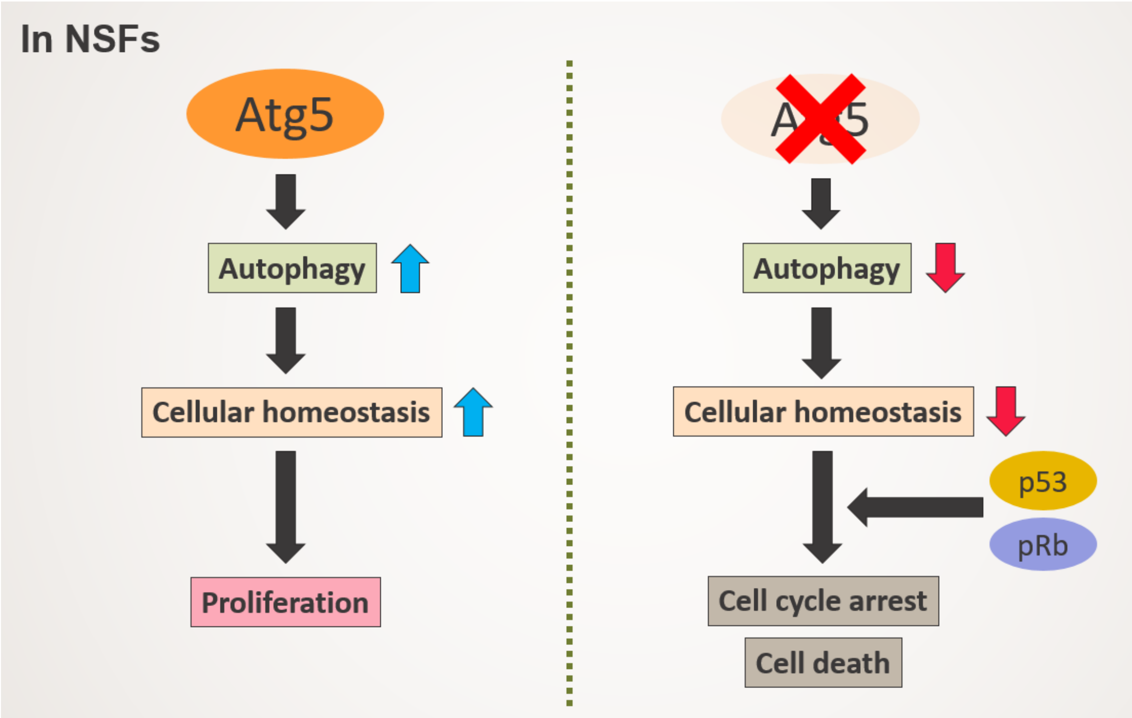

Fig. 9: Schematic model of the role of Atg5 in NSFs.

Atg5-mediated autophagy plays crucial roles in NSF proliferation and maintenance of cellular homeostasis (left); Atg5 knockdown in NSFs induces suppression of proliferation and disturb cellular homeostasis. p53/Rb pro-apoptotic pathway contributes to growth arrest and induction of apoptosis/anoikis in Atg5-depleted NSFs. (Right)

Acknowledgement

This study was carried out at Department of Oncogene Research, Research Institute for Microbial Diseases, Osaka University.

I would like to express my special appreciation to Prof. Masato Okada for his tremendous support, advice, discussions and encouragement. Without his support and encouragement, I could not have finished my Ph.D. I am deeply grateful to Dr. Shigeyuki Nada for his wonderful guidance, instruction and discussions. I am very thankful to Dr. Kentaro Kajiwara for his advices and support.

I am also grateful to Dr. Kyoko Miura (Kumamoto University) for kindly providing primary NSFs and Dr. Noboru Mizushima (University of Tokyo) for kindly providing Atg5 KO MEFs.

I would like to my thanks to Ito foundation for international education exchange and Otsuka toshimi scholarship foundation. Without their supports, I could not have finished my graduate course in Japan.

Finally, I am deeply grateful to my family, my friends and all members of Department of Oncogene Research, RIMD for help and encouragement.

Publications

<u>Junhyeong Kim</u>, Woei-Yaw Chee, Norikazu Yabuta, Kentaro Kajiwara, Shigeyuki Nada, Masato Okada. Atg5-mediated autophagy controls apoptosis/anoikis via p53/Rb pathway in naked mole-rat fibroblasts. *Biochemical and Biophysical Research Communications*, (in press).